

Tube Loss: A Novel Approach for Prediction Interval Estimation and probabilistic forecasting

Pritam Anand

DA-IICT, Gandhinagar.

pritam_anand@daiict.ac.in

Tathagata Bandyopadhyay

DA-IICT, Gandhinagar.

tathagata_b@daiict.ac.in

Suresh Chandra

Ex-faculty, IIT, Delhi.

sureshiitdelhi@gmail.com

Editor:

Abstract

This paper proposes a novel loss function, called 'Tube Loss', for simultaneous estimation of bounds of a Prediction Interval (PI) in the regression setup. The PIs obtained by minimizing the empirical risk based on the Tube Loss are shown to be of better quality than the PIs obtained by the existing methods in the following sense. First, it yields intervals that attain the prespecified confidence level $t \in (0, 1)$ asymptotically. A theoretical proof of this fact is given. Secondly, the user is allowed to move the interval up or down by controlling the value of a parameter. This helps the user to choose a PI capturing denser regions of the probability distribution of the response variable inside the interval, and thus, sharpening its width. This is shown to be especially useful when the conditional distribution of the response variable is skewed. Further, the Tube Loss based PI estimation method can trade-off between the coverage and the average width by solving a single optimization problem. It enables further reduction of the average width of PI through re-calibration. Also, unlike a few existing PI estimation methods the gradient descent (GD) method can be used for minimization of empirical risk. Through extensive experiments, we demonstrate the effectiveness of Tube Loss-based PI estimation in both kernel machines and neural networks. Additionally, we show that Tube Loss-based deep probabilistic forecasting models achieve superior performance compared to existing probabilistic forecasting techniques across several benchmark and wind datasets. Finally, we empirically validate the advantages of the Tube loss approach within the conformal prediction framework. Codes are available at https://github.com/ltpritamanand/Tube_loss.

Keywords: Uncertainty Quantification, Quantile Regression, Prediction Interval Estimation.

1 Introduction

In regression setting, machine learning (ML) algorithms predict the value of a variable y , often called dependent variable, given the value of an independent variable, say, x . Merely giving the predicted value of y without attaching a measure of uncertainty with it, may not be useful in real world applications. Uncertainty quantification (UQ) is especially important, when the cost of incorrect prediction is high. For example, in planning replacement of a critical and expensive component of a nuclear reactor, failure of which may lead to a nuclear

disaster, the information that the predicted value of its life is 2.5 years without attaching a measure of uncertainty may not be useful. In contrast, if it is predicted that the life of critical component is between 2 and 3 years with, say, 99% confidence, it throws out useful information. Such an interval, predicted for values of y , is often called a prediction interval (PI) with a pre-specified confidence (in this case 99%).

Let us assume $(x_i, y_i), i = 1, 2, \dots, m$, denote m independent copies of the random variables (x, y) having a joint distribution $p(x, y)$. With some abuse of notation, we denote by (x, y) , a pair of random variables as well as its values whenever the distinction is obvious. A standard regression model provides an estimate of $\mathbb{E}(y|x)$ as the predicted value of y . However, for uncertainty quantification (**UQ**) of the output of a Neural Network (NN) in regression setting, researchers have obtained Prediction Interval (PI) of y given x with a certain confidence (Khosravi et al. (2011b), Khosravi et al. (2011a), Nix and Weigend (1994), Pearce et al. (2018), Chung et al. (2021)). The limits of a PI are appropriately chosen quantiles of the distribution of NN outputs y given x , and are thus, naturally, functions of x . Given x , let's denote a PI of y with confidence t by $[\mu_1(x), \mu_2(x)]$ where $\mu_1(x)$ and $\mu_2(x)$ are the lower and the upper bounds of the interval, respectively, satisfying $P[\mu_1(x) \leq y \leq \mu_2(x)] \geq t$ where the probability is calculated based on the conditional distribution of y given x .

Notice that, in the set-up described above, there are infinitely many choices of the bounds $\mu_1(x)$ and $\mu_2(x)$ satisfying the coverage constraint. Among all choices, the shortest PI, the PI having minimum average width $\mathbb{E}[\mu_2(x) - \mu_1(x)]$ is preferable, where the expectation is based on the marginal distribution of x . Suppose $[\hat{\mu}_1(x), \hat{\mu}_2(x)]$ denotes an estimate of PI $[\mu_1(x), \mu_2(x)]$ based on the data $(x_i, y_i), i = 1, 2, \dots, m$, then we judge the quality of an estimated PI by two metrics. First, PI Coverage Probability (**PICP**) defined as the proportion of y_i s lying inside of the estimated interval. Naturally, we expect it to be close to t . Second, the Mean PI width (**MPIW**) defined as $\frac{1}{m} \sum_{i=1, \dots, m} [\hat{\mu}_2(x_i) - \hat{\mu}_1(x_i)]$. Among all intervals satisfying the constraint that **PICP** is greater than equal to t , the interval which minimizes **MPIW** is considered as the optimal choice of a PI. Following Pearce et al. (2018) we may call it **High Quality (HQ)** principle to be followed for choosing a PI.

However, a well-calibrated HQ PI guarantees the target coverage level t only asymptotically, and may fail to achieve it on finite test samples. In real-world decision-making, especially in high-stakes applications, guarantees on finite test samples coverage are often essential. Conformal Regression (CR) (Vovk et al. (1999, 2005)) provides a principled framework through which PI models can be adapted to ensure such finite-sample coverage guarantees, making them more suitable for practical deployment.

For quantifying the uncertainty in regression task, various NN based PI estimation approaches have been proposed in the literature. Some, like the delta method (Hwang and Ding (1997), Chryssoulouris et al. (1996)), the Mean-Variance Estimation (MVE) method (Nix and Weigend (1994)) and the Bayesian technique (MacKay (1992)) assume that the noises are independent Gaussian random variables. The PIs obtained by such methods may, thus, perform poorly, especially when the data distribution is highly skewed and/or heavy tailed. To get round this problem, some (Chung et al. (2021), Cui et al. (2020)) propose estimating $\mathbb{E}(y|x)$, and then the error distribution or its different moments. However, an alternative and a direct method for finding PI is to estimate appropriate quantiles of the conditional distribution of y given x . The q^{th} quantile of y for a given x , say, $F_q(x)$ is defined as $P(y \leq F_q(x)|x) = q, q \in (0, 1)$. Clearly, thus, an estimate of the interval $[F_q(x), F_{q+t}(x)]$

based on the training set T provides a PI with confidence t for all choices of q satisfying $q, q+t \in (0, 1)$. In other words, finding a PI with confidence t simply requires the estimation of the quantile functions $F_q(x)$ and $F_{q+t}(x)$ for a q satisfying $q, q+t \in (0, 1)$. Notice that every choice of $q \in (0, 1)$ such that $q+t \in (0, 1)$ leads to a PI with confidence t . Thus, the method of construction of PI using quantiles subsumes the constraint on **PICP**.

In non-parametric framework, an estimate of $F_q(x)$, say, $\hat{F}_q(x)$ (Takeuchi et al. (2006)) is obtained by minimizing the empirical loss using pinball loss function which we discuss in detail in the next section. Thus, the resulting PI becomes $[\hat{F}_q(x), \hat{F}_{q+t}(x)]$. Notice that, for finding the lower and upper bounds of $[\hat{F}_q(x), \hat{F}_{q+t}(x)]$, the pinball loss minimization problem is to be solved independently for q and $q+t$. Further, for finding a **HQ** PI, one needs to search for a q among all feasible choices that minimizes the **MPIW** $\frac{1}{m} \sum_{i=1, \dots, m} [\hat{F}_{q+t}(x_i) - \hat{F}_q(x_i)]$. This amounts to solving two separate optimization problems repeatedly searching across all feasible choices of q . Consequently, PI estimation through this approach becomes computationally expensive. The question that naturally arises, whether the lower and upper bounds of a PI can be estimated simultaneously requiring solution of a single optimization problem.

Recently, in regression setting with Neural Network (NN), Khosravi et al. propose a solution to this problem by formulating Lower and Upper Bound Estimation (LUBE) (Khosravi et al. (2011a)) as a single constrained optimization problem. LUBE searches for a PI that minimizes a loss function which is a non-linear function **PICP** and **MPIW**. However, to minimize the loss of LUBE, the gradient descent (GD) method cannot be used as it involves **PICP**, a step function whose derivative is zero almost everywhere. This is inconvenient considering that GD is the standard method for training NN. To train LUBE NN (Khosravi et al. (2011a)), thus, Khosravi et al. have used simulated annealing (SA), a non-gradient based optimization method. Latter researchers use other non-gradient based training methods, like Genetic Algorithms (Ak et al., 2013), Gravitational Search Algorithms (Lian et al., 2016), PSO (Galvan et al., 2017, Wang et al., 2017), and Artificial Bee Colony Algorithms (Shen et al., 2018).

Pearce et al. (2018) simplify the LUBE loss function by considering a linear combination of **MPIW** and $\max(0, t - \text{PICP})^2$ which they name Quality-Driven (QD) distribution-free loss function. However, to enable the use of GD method in training NN they propose approximating **PICP**, a step function, by the product of two sigmoid functions. Unlike (Khosravi et al. (2011a)), they incorporate the model uncertainty in PI estimation using an ensemble method.

The above methods for simultaneous estimation of PI bounds are based on the **HQ** principle. However, these methods fail to guarantee the target confidence t asymptotically. In contrast, the quantile-based prediction interval (PI) estimation method is specifically designed to achieve the target confidence level. However, estimating the bounds $\hat{F}_q(x)$ and $\hat{F}_{q+t}(x)$ typically requires solving two separate and independent pinball loss minimization problems, each with parameters q and $q+t$, respectively. This approach introduces two major challenges. First, as previously discussed, it significantly increases computational complexity, particularly when learning with complex neural network architectures and large-scale datasets. Second, it can not explicitly minimize the width of the PI within the optimization process for obtaining the narrower PI in practice.

In this work, we introduce Tube Loss, a novel loss function, for the PI estimation, probabilistic forecasting and conformal regression tasks. The motivation behind introducing it is to yield estimates of the two quantile bounds simultaneously by solving a single optimization problem. In the following, we highlight the interesting properties of the Tube loss function.

- (i) The minimizer of the empirical risk based on Tube loss is a pair of functions $(\hat{\mu}_1(x), \hat{\mu}_2(x))$ yielding the PI $[\hat{\mu}_1(x), \hat{\mu}_2(x)]$ which attains the target confidence t asymptotically. We have provided a theoretical proof of this statement. This property makes it a natural choice for the loss function to be used in PI estimation and probabilistic forecasting.
- (ii) For minimizing the average width of a PI with a prespecified confidence t , the PI needs to capture denser regions of the distributions of y given x . To achieve it, we introduce an additional parameter r in Tube loss function. By adjusting the value of r , the PI bounds can be moved up or down maintaining the coverage. Thus, a proper choice of r enables capturing denser region of the y values for each x . This is found to be very effective in reducing the width of the PI especially when the distribution of $y|x$ is skewed. For symmetric distribution, however $r = 0.5$ is the default choice resulting a centered PI.
- (iii) The Tube loss function is differentiable almost everywhere (re Lebesgue measure) with non-zero gradients. It enables direct application of GD method for minimization of average Tube loss in different neural architectures. As discussed above, GD cannot be used for PI estimation using LUBE loss. Further, for enabling use of GD in PI estimation using QD loss, the step function in QD loss is approximated by a smooth function. It is evident from the experimental results in Section 3 that the quality of PI depends on the quality of approximation of the step function. In contrast, GD method is used without encountering any problem for training of Tube loss based learning models.
- (iv) The Tube loss based PI estimation method allows trading off over-coverage for average width by introducing a user defined parameter δ in the optimization problem. The default choice of δ is zero. But, often in some experiments we observe that the Tube loss-based PI achieves empirical coverage higher than the target t on the validation set. In such cases, the average width of the PI on the test set can be further reduced by retraining the model (a process termed as *re-calibration*) with a smaller non zero value of δ .

As compared to the quantile approach, the Tube loss approach significantly reduces the overall complexity of the PI estimation, probabilistic forecasting and conformal regression tasks. It is because that unlike the quantile approach, the Tube loss approach can simultaneously estimate the pair of quantile functions by training a single model.

In this paper, we perform an extensive set of experiments to show the efficacy of the Tube loss approach. At first, we perform several experiments to outline the advantages of the Tube loss function in kernel machine and neural network for PI estimation tasks. Next, we employ the Tube loss function in different deep forecasting architectures for probabilistic forecasting tasks and show that the Tube loss based deep learning

models outperform the existing probabilistic forecasting models on several benchmark and wind speed datasets. At last, we extend the Tube loss approach in conformal regression (Vovk et al. (1999)) setting as well.

The remainder of the paper is organized as follows. Section 2 introduces the necessary mathematical preliminaries. Section 3 reviews related work on PI estimation, probabilistic forecasting, and conformal regression. Section 4 introduces the Tube loss function by outlining its key properties, its application in kernel machine and NN for PI estimation task and extensions to probabilistic forecasting and conformal regression. Section 5 details the experimental setup and results through extensive numerical evaluations. Finally, Section 6 concludes the paper with a summary of key findings and future directions.

2 Notations & Mathematical Preliminaries

Let \mathcal{X} and \mathcal{Y} denote the domains of x and y , respectively. In most applications $\mathcal{X} = \mathbb{R}^n$ and $\mathcal{Y} = \mathbb{R}$, where \mathbb{R} is the set of real numbers. Let $T = \{(x_i, y_i) : x_i \in \mathcal{X}, y_i \in \mathcal{Y}, i = 1, 2, \dots, m\}$ be the training set, where $(x_i, y_i), i = 1, 2, \dots, m$ are independently and identically distributed (iid) random variables having a joint distribution $p(x, y)$. With some abuse of notation, we denote by (x, y) , a pair of random variables as well as its values whenever the distinction is obvious.

In non-parametric framework, an estimate of $F_q(x)$, say, $\hat{F}_q(x)$ based on the training set T is given by

$$\hat{F}_q(x) = \arg \min_{\mu} \sum_i \rho_q(y_i - \mu(x_i)), \quad (1)$$

where, $\mu(\cdot)$ belongs to a suitably chosen class of functions. And $\rho_q(u)$, the pinball loss function (Koenker and Bassett Jr (1978), Koenker and Hallock (2001)), is given by (Figure 1)

$$\rho_q(u) = \begin{cases} qu, & \text{if } u \geq 0, \\ (q-1)u, & \text{otherwise.} \end{cases} \quad (2)$$

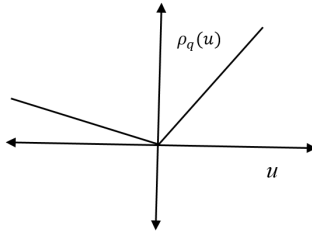


Figure 1: Pinball loss

Takeuchi et al. (2006) prove that for large m if the conditional distribution of y given x does not contain any discrete component, the proportion of y_i 's below $\hat{F}_q(x)$ across all values of x converges to q . Thus, for large m and fixed q such that $q + t \leq 1$, $[\hat{F}_q(x), \hat{F}_{q+t}(x)]$ provides a PI of y with confidence t . However, for finding $\hat{F}_q(x)$ and $\hat{F}_{q+t}(x)$ one needs to

solve the above optimization problem independently for q and $q + t$. Further, for finding a HQ PI, among all feasible choices one needs to search for a q such that the mean prediction interval width (MPIW) given by $m^{-1} \sum_i (\hat{F}_{q+t}(x_i) - \hat{F}_q(x_i))$ is minimized. This amounts to solving two separate optimization problems repeatedly across feasible choices of q . Evidently, the PI estimation through this approach is computationally expensive.

Instead of estimating the bounds separately, the lower and upper quantile bounds of the PI, $[\mu_1(x), \mu_2(x)]$ was simultaneously obtained by (Khosravi et al. (2011a)) first in distribution-free setting. They proposed finding the estimates of $\mu_1(x)$ and $\mu_2(x)$ simultaneously by minimizing the novel LUBE loss function (Khosravi et al. (2011a)). Thereafter, (Pearce et al. (2018)) improved the LUBE loss by developing the Quality Driven (QD) loss function. The LUBE and QD loss function based PI models are direct PI estimation models as they can obtain the lower and upper quantile bounds of the PI simultaneously.

Let $[\hat{\mu}_1(x), \hat{\mu}_2(x)]$ be the estimated PI on training set (x_i, y_i) , $i = 1, 2, \dots, m$. Then, its empirical coverage (PICP), and mean width (MPIW) are defined as

$$PICP = m^{-1} \sum_{i=1,2,\dots,m} k_i, \quad (3)$$

where,

$$k_i = \begin{cases} 1, & \text{if } y_i \in [\hat{\mu}_1(x), \hat{\mu}_2(x)], \\ 0, & \text{Otherwise,} \end{cases} \quad (4)$$

and

$$MPIW = m^{-1} \sum_{i=1,2,\dots,m} [\hat{\mu}_2(x_i) - \hat{\mu}_1(x_i)], \quad (5)$$

respectively.

The LUBE and QD loss functions both considers the minimization of the non-linear functions of PICP and MPIW for achieving the narrower PI.

3 Related Works

In this section, we summarize some important and relevant methods developed for PI estimation and probabilistic forecasting.

3.1 PI estimation in Kernel Machines

In kernel machine literature, the PI is commonly estimated through the quantile approach. For given $0 < q, q + t < 1$, the bounds of the PI, $\hat{F}_q(x)$ and $\hat{F}_{q+t}(x)$ are kernel generated functions. For estimation of τ^{th} quantile function $\hat{F}_\tau(x)$, SVM model requires the solution to the following optimization problem

$$\min_{(\alpha, \alpha_0)} \left[\frac{\lambda}{2} \alpha^T \alpha + \frac{1}{m} \sum_{i=1}^m \rho_\tau(y_i - (K(A^T, x_i) \alpha + \alpha_0)) \right] \quad (6)$$

where, $\rho_\tau(u)$ is as defined in (2), $K(A^T, x) = [k(x_1, x), k(x_2, x), \dots, k(x_m, x)]$ and $k(x, y)$ is a positive semi-definite kernel (Mercer (1909)). Clearly, for the estimation of PI with

confidence t , the problem (6) needs to be solved independently for $\tau = q$ and $\tau = q + t$, respectively for a suitable choice of q .

3.2 PI estimation in Neural Networks

The PI estimation problem in NN framework has been well studied. Some of the commonly used methods are the Delta Method Papadopoulos et al. (2001) Khosravi et al. (2011b), Bayesian Method Ungar et al. (1996) and Mean Variance Estimation (MVE) Method Nix and Weigend (1994). A systematic and detailed description of these methods can be found at Kabir et al. (2018). But, all these methods assume Gaussian noise distribution and thus, fail to ensure a consistent performance on a variety of data sets.

Khosravi et al. (2011) first propose direct PI method for simultaneous estimation of lower and upper bounds of a PI in the distribution-free setting by introducing the LUBE loss (Khosravi et al. (2011a)), given by

$$LUBE = NMPIW(1 + \gamma(PICP)e^{-\eta(PICP-t)}). \quad (7)$$

where, $NMPIW(= \frac{MPIW}{R})$, $R(= \max(y_i) - \min(y_i))$ is the range of response values y_i and η is a user-defined parameter can be used to magnify any small difference between $PICP$ and t , and $\gamma(PICP) = 0$, if $PICP \geq t$ and 1, otherwise.

Khosravi et al. (2011) describes that the LUBE loss function is “nonlinear, complex and non differentiable.” As a consequence, the GD method cannot be applied for its minimization. Also, the sub-gradients of the loss function are zero almost everywhere. They propose simulated annealing (SA), a non-gradient based method, for training the LUBE NN. Though SA was originally proposed as the training method, later various other non-gradient based methods are used for training the LUBE NN, including Genetic Algorithms (AK et al., 2013), Gravitational Search Algorithms (Lian et al. 2016), PSO (Galvan et al., 2017), and Artificial Bee Colony Algorithms (Shen et al, 2018).

LUBE has been extensively used by the researchers in various application-focused work, like energy load predictions (Pinson and Kariniotakis, 2013; Quan et al., 2014), wind speed forecasting (Wang et al., 2017, Ak et al., 2013), prediction of landslide displacement (Lian et al., 2016), gas flow (Sun et al., 2017) and solar energy (Galvan et al., 2017).

As discussed above, a major drawback of PI estimation using LUBE is, GD method cannot be used for its minimization. This is inconvenient considering that GD is now the standard method for training NNs. To overcome this problem, Pearce et al. (2018) building up on the same logic as (Khosravi et al. (2011a)), propose the QD loss function, given by

$$Loss_{QD} = MPIW_{capt.} + \lambda \frac{m}{t(1-t)} \max(0, (t - PICP))^2, \quad (8)$$

where $MPIW_{capt.} = \frac{\sum_{i=1}^m (\hat{\mu}_2(x_i) - \hat{\mu}_1(x_i)) \cdot k_i}{\sum_{i=1}^m k_i}$, k_i is as defined in (4) and λ is the user-defined trade-off parameter. Notice that in contrast to $MPIW$, $MPIW_{capt.}$ captures the average width for those points lying inside the PI. As explained in Section 3.3.1 of (Pearce et al. (2018)), like LUBE, $Loss_{QD}$ cannot be minimized directly using GD method since the derivative of the step function $PICP$ is zero almost everywhere. To remediate this and thus, enabling the use of GD method for minimization, they propose approximating the step function by the product of two sigmoid functions which has been used previously by

Yan et al. (2004). They also propose using an ensemble of NN models instead of a single NN. The new model is found to yield PIs with shorter average widths. One practical issue encountered during the training of the QD NN is that the gradient values tend to approach infinity when the lower bound of the PI crosses its upper bound during some gradient descent iterations. This leads to poor-quality PI. For stabilizing the training process of NN, Salem et al. introduced a penalty term in the QD loss function to enforce the consistency of the PI bounds in their work (Salem et al. (2020)) and named this modification as the QD^+ loss function.

It is worth noting that both the LUBE and QD loss functions are specifically designed to jointly minimize the average width of the prediction interval ($MPIW$ or $MPIW_{capt.}$) and the coverage error. The coverage error quantifies the extent to which the empirical coverage achieved by the PI model misses the target t . However, there are two major concerns with the LUBE and QD loss function based PI models. First, none of these methods guarantees PI to converge to the target coverage t as the sample size becomes large. Second, unlike the quantile based method, they fail to facilitate the movement of the PI tube. The movement of the PI tube is a natural and implicit way to reduce the width of the PI by ensuring that the PI crosses through the denser region of the data cloud. It is particularly very useful when the data distribution is skewed. Our proposed Tube loss function addresses these two major issues associated with the LUBE and QD loss based PI models described above.

3.3 Probabilistic Forecasting in Deep Network

The probabilistic forecasting is basically a PI estimation task in auto-regressive setting. Given the time-series data $\{y_t, t = 1, 2, \dots, m\}$ on a variable y over m time points and a lag window $p \leq m$, the probabilistic forecasting models obtain the PI for y_{i+1} using the features $z_i = (y_i, y_{i-1}, \dots, y_{i-p+1})$ for $i \geq m$ with given target coverage t . The bounds of the PI are basically the estimates of q^{th} and $(t + q)^{th}$ quantiles of the distribution $(y_{i+1}|z_i)$, $i \geq p$, for some positive q satisfying $t + q \leq 1$.

Similar to the prediction interval (PI) literature, probabilistic forecasting methods have been developed within two widely adopted frameworks. In the parametric framework, the joint distribution of $\{y_t, t = 1, 2, \dots, m\}$ is assumed to be multivariate normal with some kind of dependence structure. Consequently, the conditional distribution of $(y_{i+1}|z_i)$ is normal with mean $\mu(z_i)$ and standard deviation $\sigma(z_i)$. The output layer of the deep network produces the maximum likelihood estimates of the mean and the standard deviation of the conditional distribution $(y_{i+1}|z_i)$. Often, the normality assumption is based on mathematical convenience rather than evidence, which is often not adequate Gasthaus et al. (2019) for addressing the PI estimation problem.

One popular class of the probabilistic forecasting models is Mixture Density Network (MDN) which assumes that the conditional distribution $(y_{i+1}|z_i)$ is the mixture of k normal distribution. The task of deep learning network is to estimate the mean μ_i , standard deviation σ_i and mixing coefficient π_i for $i = 1, 2, \dots, k$. The MDN-based deep learning architectures have been used for probabilistic forecasting of wind speed (Zhang et al. (2020)) and electric load (Afrasiabi et al. (2020)). Other popular probabilistic forecasting algorithm is Deep AR (Salinas et al. (2020)), which can also efficiently incorporate the co-variate time-series data in order to capture the complex, group-dependent behavior. Apart from the normal noise

model, it can also consider the negative binomial noise model for probabilistic forecasting. Deep AR model has been applied for effective probabilistic forecast of wind speed in (Arora et al. (2022)).

In the literature, Quantile based probabilistic forecasting models are among the most widely used approaches. They have been applied across various domains including wind power forecasting (Yu et al. (2021)), electric load forecasting (Zhang et al. (2018); Xu and Chen (2024); Wang et al. (2019)), and solar forecasting (Panamtaash and Zhou (2018)) to produce high-quality probabilistic forecasts. Quantile-based probabilistic forecasting models are distribution-free, which allows them to achieve consistent performance across a wide variety of data distributions and application domains.

Similar to the PI estimation task, the deep probabilistic forecasting task through quantile approach is a two stage process. At first, for given $0 \leq q + t \leq 1$, we train a deep auto-regressive forecasting architecture such as LSTM, GRU or TCN for obtaining the q^{th} quantile of the distribution $(y_{i+1}|z_i)$ by solving the problem

$$\min_{(\mu_1)} \sum_{i=p}^{m-1} \rho_q(x_{i+1} - \mu_1(z_i)), \quad (9)$$

where $\mu_1(z_i)$ corresponds to the output layer node of the used deep auto-regressive architecture and $\rho_q(u)$ is the pinball loss function detailed in (1). The output as well as hidden layer weights of the used deep auto-regressive architecture is optimized by back-propagating the error (9) throughout the network. Thereafter, we train another deep auto-regressive forecasting architecture for obtaining the $(q + t)^{th}$ quantile of the distribution $(y_{i+1}|z_i)$ by solving the problem

$$\min_{(\mu_2)} \sum_{i=p}^{m-1} \rho_{q+t}(x_{i+1} - \mu_2(z_i)), \quad (10)$$

After training two separate deep architectures to solve the optimization problems (9) and (10), respectively, the prediction interval (PI) for the future observation x_{m+1} is estimated as $[\hat{\mu}_1(z_m), \hat{\mu}_2(z_m)]$.

Modern deep forecasting models tend to be complex, especially when applied to large-scale datasets. Quantile-based deep probabilistic forecasting models require the training of two separate deep learning models, which further increases the overall complexity of the forecasting task. Moreover, these models do not explicitly minimize the PI width to ensure narrower intervals for future observations. Tube-loss-based deep probabilistic forecasting models address these limitation by reducing the complexity inherent in quantile-based approaches and produce the PI with lower MPIW.

3.4 Conformal Regression

The PI estimation models are expected to estimate the PI such that it guarantees the target calibration asymptotically with lesser possible width. However, real-world decision-making often requires this guarantee to hold on finite test samples, not just only in the asymptotic sense. The Conformal Regression (CR) (Vovk et al. (1999, 2005)) is a general methodology which can adjust the PI to obtain the non-asymptomatic coverage guarantee on finite test sample under very general data exchangeability assumption.

The split CR procedure (Papadopoulos et al. (2001); Papadopoulos (2008)) begins by partitioning the training set T into two disjoint subsets: a calibration set I_2 , and the remaining set I_1 , which is used for model training. Next, a nonconformity score function is defined to quantify the discrepancy between the predicted value of y_i , obtained from the learning model, and its true value, for a given input x_i . The non-conformity score is computed on the calibration set I_2 . One of the most obvious choice of the non-conformity score is absolute residual value which is computed by

$$R = |y_i - \hat{f}(x_i)|, \quad i \in I_2, \quad (11)$$

where \hat{f} is the estimate of the mean regression model trained on I_1 . For the target calibration t , a quantile of the empirical distribution of absolute residuals is computed by

$$Q_t(R, I_2) = t(1 + \frac{1}{I_2})\text{-th empirical quantile of } \{R_i : i \in I_2\} \quad (12)$$

and the prediction set for new test point x_{m+1} is obtained by

$$C(x_{m+1}) = [\hat{f}(x_{m+1}) - Q_t(R, I_2), \hat{f}(x_{m+1}) + Q_t(R, I_2)] \quad (13)$$

The prediction set $C(x_{m+1})$ is guaranteed to satisfy

$$P(y_{m+1} \in C(x_{m+1})) \geq t \quad (14)$$

for any joint distribution $p(x, y)$ with the assumption that the samples in set $\{(x_i, y_i) : x_i \in \mathcal{X}, y_i \in \mathcal{Y}, i = 1, 2, \dots, m\}$ are exchangeable. A detail study is presented in (Angelopoulos et al. (2024)).

One of the problem with the conformal prediction set obtained through the absolute residual nonconformity score (11) is that the length of the prediction set $C(x_{m+1})$ remains fixed and independent of x_{m+1} . Romano et al. have developed the quantile regression based nonconformity score and obtained the fully adaptive conformal prediction set in their work Conformalized Quantile Regression (CQR) (Romano et al. (2019)). In NN framework, the CQR method first requires the training of the two independent network each of them minimizing pinball loss for estimating the q^{th} or $(q + t)^{th}$ quantile function on set I_1 for some $0 \leq q, q + t \leq 1$. Let the q^{th} and $(q + t)^{th}$ quantile function estimated on the set I_1 is $\hat{F}_{lo}(x)$ and $\hat{F}_{hi}(x)$ respectively then, the CQR model computes the non-conformity score E_i on calibration set I_2 using

$$E_i = \max\{\hat{F}_{lo}(x) - y_i, y_i - \hat{F}_{hi}(x)\}. \quad (15)$$

Thereafter, following the conformal methodology, the $Q_t(E, I_2) = t(1 + \frac{1}{I_2})$ -th empirical quantile of $\{E_i : i \in I_2\}$ is computed and adaptive prediction set on new test point x_{m+1} is obtained by

$$C(x_{m+1}) = [\hat{F}_{lo}(x_{m+1}) - Q_t(E, I_2), \hat{F}_{hi}(x_{m+1}) + Q_t(E, I_2)] \quad (16)$$

Similar to the PI estimation task, the computation of the nonconformity scores in CQR requires the training of the two independent NN for estimating the two quantile bound

function of the PI \hat{F}_{lo} and $\hat{F}_{hi}(x)$ one by one. It makes the overall CR task complex particularly when the set I_1 is large. Our Tube loss model simplifies the CQR process by estimating the functions $\hat{F}_{lo}(x)$ and $\hat{F}_{hi}(x)$ simultaneously by training a single network. Our numerical results demonstrate that the Tube loss-based CR method achieves approximately a 50% reduction in overall computational time compared to the CQR model, without compromising the quality of the prediction set.

4 Tube Loss function

For a given $t \in (0, 1)$ and $u_2 \leq u_1$, we define the Tube loss function as

$$\rho_t^r(u_2, u_1) = \begin{cases} tu_2, & \text{if } u_2 > 0, \\ -(1-t)u_2, & \text{if } u_2 \leq 0, u_1 \geq 0 \text{ and } ru_2 + (1-r)u_1 \geq 0, \\ (1-t)u_1, & \text{if } u_2 \leq 0, u_1 \geq 0 \text{ and } ru_2 + (1-r)u_1 < 0, \\ -tu_1, & \text{if } u_1 < 0, \end{cases} \quad (17)$$

where $0 < r < 1$ is a user-defined parameter and (u_2, u_1) are errors, representing the deviations of y values from the bounds of PI.

The Tube loss function is a function of two variables. In Figure 2, plots of the Tube loss are given for $r = 0.5$. For $r = 0.5$, $\rho_t^r(u_1, u_2)$ is symmetrically located around the line $u_1 + u_2 = 0$ and **continuous function** of (u_1, u_2) . The default choice of r in the Tube loss function is 0.5 which targets to obtain the centered PI. The centered PI is expected to obtain the lesser width, if the distribution of $y|x$ is symmetric. However, this is not the case of asymmetric distribution.

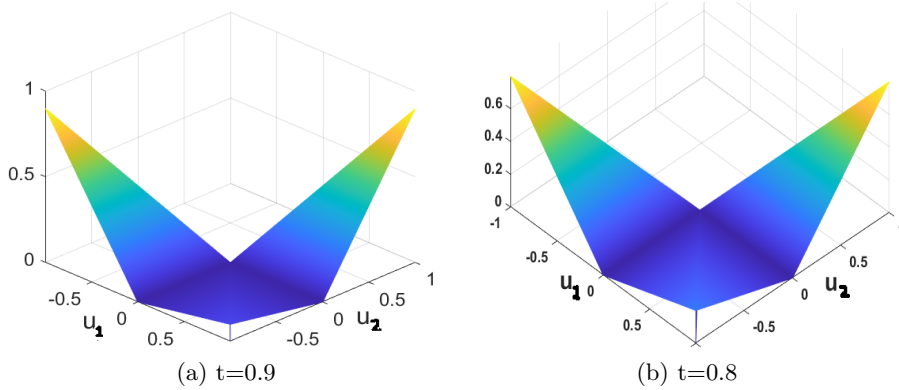


Figure 2: Tube loss function

To provide better intuition, we replace u_1 by $y - \mu_1$ and u_2 by $y - \mu_2$. The Tube loss function then reduces to

$$\rho_t^r(y, \mu_1, \mu_2) = \begin{cases} t(y - \mu_2), & \text{if } y > \mu_2. \\ (1-t)(\mu_2 - y), & \text{if } \mu_1 \leq y \leq \mu_2 \text{ and } y \geq r\mu_2 + (1-r)\mu_1, \\ (1-t)(y - \mu_1), & \text{if } \mu_1 \leq y \leq \mu_2 \text{ and } y < r\mu_2 + (1-r)\mu_1, \\ t(\mu_1 - y), & \text{if } y < \mu_1, \end{cases} \quad (18)$$

For given (x_i, y_i) , $i = 1, 2, \dots, m$, and a confidence level $t \in (0, 1)$, the PI $[\hat{\mu}_1(x), \hat{\mu}_2(x)]$ is the solution of the following optimization problem

$$\arg \min_{\mu_1, \mu_2} \sum_{i=1}^m \rho_t^r(y_i, \mu_1(x_i), \mu_2(x_i)), \quad (19)$$

where, $\mu_1(\cdot)$ and $\mu_2(\cdot)$ belong to a suitably chosen class of functions and $\rho_t^r(y, \mu_1(x), \mu_2(x))$, is given by

$$\rho_t^r(y, \mu_1(x), \mu_2(x)) = \begin{cases} t(y - \mu_2(x)), & \text{if } y > \mu_2(x). \\ (1-t)(\mu_2(x) - y), & \text{if } \mu_1(x) \leq y \leq \mu_2(x) \text{ and } y \geq r\mu_2(x) + (1-r)\mu_1(x). \\ (1-t)(y - \mu_1(x)), & \text{if } \mu_1(x) \leq y \leq \mu_2(x) \text{ and } y < r\mu_2(x) + (1-r)\mu_1(x). \\ t(\mu_1(x) - y), & \text{if } y < \mu_1(x). \end{cases} \quad (20)$$

By controlling the value of the user parameter $0 < r < 1$, the upper and lower bounds of the PI could be moved up and down simultaneously. This is a consequence of Proposition 1 discussed in detail in Sub-section 4.1. From Figure 5 (cf. Section 5), it is evident that with increase in the value of r the upper and the lower bounds of PI move up simultaneously. As stated above, an appropriate choice of r may, thus, help in reducing MPIW by capturing denser regions of data cloud, especially when the conditional distributions of y given x across different values of x are skewed.

4.1 Asymptotic properties of the Tube loss function

Let y_1, y_2, \dots, y_m be iid following the distribution of a continuous random variable Y and $t \in (0, 1)$. Let us define the following subsets of \mathbb{R} : $\mathfrak{R}_1(\mu_1, \mu_2) = \{y : y > \mu_2\}$, $\mathfrak{R}_2(\mu_1, \mu_2) = \{y : \mu_1 < y < \mu_2, y > r\mu_2 + (1-r)\mu_1\}$, $\mathfrak{R}_3(\mu_1, \mu_2) = \{y : \mu_1 < y < \mu_2, y < r\mu_2 + (1-r)\mu_1\}$ and $\mathfrak{R}_4(\mu_1, \mu_2) = \{y : y < \mu_1\}$. Notice that the sets $\mathfrak{R}_i(\mu_1, \mu_2)$, $i = 1, 2, 3, 4$ are so defined that they do not include the points on the boundaries. Suppose (μ_1^*, μ_2^*) is the minimizer of $\frac{1}{m} \sum_{i=1}^m \rho_t^r(y_i, \mu_1, \mu_2)$ with respect to (μ_1, μ_2) , and m_k denotes the number of data points in $\mathfrak{R}_k(\mu_1^*, \mu_2^*)$. Then we have the following lemma.

Lemma 1 *As $m \rightarrow \infty$, with probability 1 the following results hold:*

$$(i) \frac{m_1}{m_2} \rightarrow \frac{1-t}{t}, \quad (ii) \frac{m_4}{m_3} \rightarrow \frac{1-t}{t}, \quad \text{and} \quad (iii) \frac{m_1+m_4}{m_2+m_3} \rightarrow \frac{1-t}{t}.$$

The proof of the lemma is given in Appendix A.

We now extend the above lemma to the regression setup. For the training set T , let $(\hat{\mu}_1(x), \hat{\mu}_2(x))$ be the minimizer of the empirical risk $\frac{1}{m} \sum_{i=1}^m \rho_t^r(y_i, \mu_1(x_i), \mu_2(x_i))$, where $\mu_1(x)$ and $\mu_2(x)$ belong to an appropriately chosen class of functions. With some abuse of notation, we let m_k denote the cardinality of the set $\mathfrak{R}_k(\hat{\mu}_1(x), \hat{\mu}_2(x))$ ($k = 1, 2, 3, 4$) inducing a partition of the feature space (as shown in Figure 3). We then have the following proposition.

Proposition 2 *For $t \in (0, 1)$ as $m \rightarrow \infty$ the following results hold with probability 1,*

$$(i) \frac{m_1}{m_2} \rightarrow \frac{1-t}{t}, \quad (ii) \frac{m_4}{m_3} \rightarrow \frac{1-t}{t} \quad (iii) \frac{m_1+m_4}{m_2+m_3} \rightarrow \frac{1-t}{t}, \quad \text{provided } (x_i, y_i), i = 1, 2, \dots, m \text{ are iid}$$

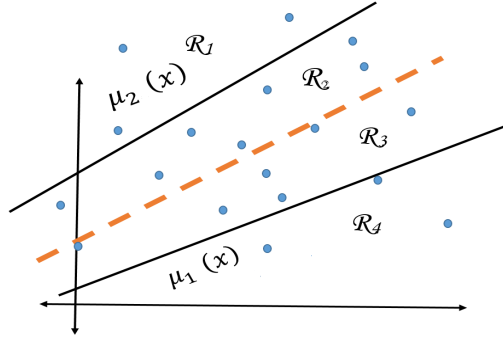


Figure 3: PI tube loss, red line represents the convex combination of $\mu_1(x)$ and $\mu_2(x)$, i.e., $r\mu_1(x) + (1-r)\mu_2(x)$, $0 < r < 1$. Blue dots represent data points (x_i, y_i) , $i = 1, 2, \dots, m$.

following a distribution $p(x, y)$ with $p(y|x)$ continuous and the expectation of the modulus of absolute continuity of its density ¹ satisfies $\lim_{\delta \rightarrow 0} E[\epsilon(\delta)] = 0$.

Proof: The proof follows from the proof of the Lemma stated above and Lemma 3 of Takeuchi et al. (2006).

4.2 The r parameter and movement of the PI bounds

Now, we show that how the PI tube can be moved up and down by choosing r appropriately in the Tube loss function.

Let us suppose that $(\hat{\mu}_1^{r_2}(x), \hat{\mu}_2^{r_2}(x))$ is the minimizer of the average loss for $r = r_2$ i.e. of $\frac{1}{m} \sum_{i=1}^m \rho_t^{r_2}(y_i, \mu_1(x_i), \mu_2(x_i))$. Also, we assume that there are $m_k^{r_2}$ points in the set $\mathcal{R}_k(\hat{\mu}_1^{r_2}(x), \hat{\mu}_2^{r_2}(x))$, $(k = 1, 2, 3, 4)$. Similarly, for $r = r_1 (< r_2)$, we assume that $(\hat{\mu}_1^{r_1}(x), \hat{\mu}_2^{r_1}(x))$ is the minimizer of the average loss, and there are $m_k^{r_1}$ points in the set $\mathcal{R}_k(\hat{\mu}_1^{r_1}(x), \hat{\mu}_2^{r_1}(x))$, $(k = 1, 2, 3, 4)$. Now, Proposition 1 (iii) entails that asymptotically t fraction of y values should lie inside each of the PIs $[\hat{\mu}_1^{r_1}(x), \hat{\mu}_2^{r_1}(x)]$ and $[\hat{\mu}_1^{r_2}(x), \hat{\mu}_2^{r_2}(x)]$. Since $r_1 < r_2$, (i) and (ii) of Proposition 1 entail $\frac{m_2^{r_1}}{m_3^{r_1}} > \frac{m_2^{r_2}}{m_3^{r_2}}$, which in turn implies $\frac{m_1^{r_1}}{m_4^{r_1}} > \frac{m_1^{r_2}}{m_4^{r_2}}$ asymptotically for large m . In other words, changing r from r_1 to r_2 moves the tube down. Thus, the PI bounds can be moved up and down by changing r .

As stated above, by controlling r MPIW can be reduced. But, the Tube loss function $\rho_t^r(u_1, u_2)$ is discontinuous at the separating plane $\{(u_1, u_2) : ru_2 + (1-r)u_1 = 0\}$ when $r \neq 0.5$. It is worth mentioning here that this discontinuity is not found to cause any problem in the implementation of GD method in the practical experiments as the Tube loss function is differentiable everywhere (re Lebesgue measure) with non-zero gradients.

1. The modulus of absolute continuity of a function f is defined as the function $\epsilon(\delta) = \sup \sum_i |f(b_i) - f(a_i)|$, where the supremum is taken over all disjoint intervals (a_i, b_i) with $a_i < b_i$ satisfying $\sum_i (b_i - a_i) < \delta$. Loosely speaking the conditional density $p(y|x)$ is absolutely continuous on average. This ensures that the probability of a point lying on the boundaries of PI vanishes.

4.3 Tube loss in kernel machine and Neural Network

The Tube loss PI estimation models enjoy the explicit minimization of the PI width against the empirical coverage with a user defined positive parameter δ as follows.

$$\min_{(\mu_1, \mu_2)} \left[\sum_{i=1}^m \rho_t^r(y_i, \mu_1(x_i), \mu_2(x_i)) + \delta \sum_{i=1}^m |(\mu_2(x_i) - \mu_1(x_i))| \right]. \quad (21)$$

For NN training, $(\mu_1(x), \mu_2(x))$ corresponds to two distinct neurons in the output layer of the dense network. The weights of the hidden and output layers are optimized by back-propagating the error defined in (21). In kernel machine, the Tube loss PI model estimates pair of functions

$$\mu_2(x) := \sum_{i=1}^m k(x_i, x) \alpha_i + b_1 \quad \text{and} \quad \mu_1(x) := \sum_{i=1}^m k(x_i, x) \beta_i + b_2. \quad (22)$$

where $k(x, y)$ is positive definite kernel (Mercer (1909)). For the sake of simplicity, we rewrite $\mu_1(x)$ and $\mu_2(x)$ in vector form

$$\mu_1(x) := K(A^T, x) \alpha + b_1 \quad \text{and} \quad \mu_2(x) := K(A^T, x) \beta + b_2, \quad (23)$$

where A is the $m \times n$ data matrix containing m training points in \mathbb{R}^n , $\alpha = \begin{bmatrix} \alpha_1 \\ \alpha_2 \\ \vdots \\ \alpha_m \end{bmatrix}$, $\beta =$

$\begin{bmatrix} \beta_1 \\ \beta_2 \\ \vdots \\ \beta_m \end{bmatrix}$ and $K(A^T, x) = [k(x_1, x), k(x_2, x), \dots, k(x_m, x)]$. The Tube loss based kernel machine considers the problem

$$\begin{aligned} \min_{(\alpha, \beta, b_1, b_2)} & \frac{\lambda}{2} (\alpha^T \alpha + \beta^T \beta) + \sum_{i=1}^m \rho_t^r(y_i, (K(A^T, x_i) \alpha + b_1), (K(A^T, x_i) \beta + b_2)) \\ & + \delta \sum_{i=1}^m |(K(A^T, x_i) (\alpha - \beta) + (b_1 - b_2))|. \end{aligned} \quad (24)$$

The Gradient descent solution for the Tube loss problem (24) is derived in the Appendix B.

For the High Quality PI, the value of the parameter r and δ of problem (21) should be tuned efficiently on validation set. A practical approach for selecting the value of r is to choose it from the discrete set $\{0.1, 0.2, \dots, 1\}$. The default choice of the r parameter is 0.5 which targets to estimate the centered PI.

We now design a heuristic approach for tuning the parameters of the Tube loss optimization problem (21). The parameter δ in (21) is initially set to zero, based on the theoretical justification that the minimizer of the Tube loss problem (19) ensures the desired calibration for sufficiently large values of m .

To identify the narrowest PI that meets the target coverage t , we adjust the PI through local movement by tuning the parameter r on the validation set. If the empirical coverage achieved exceeds the target t by a significant margin, this indicates potential to further narrow the PI. In such cases, we increment the parameter δ slightly and retrain the PI model (21). This process is repeated until the resulting PI on the validation set is well-calibrated to the target coverage. We refer to this iterative refinement as *recalibration*. Our numerical results show that the Tube loss-based model can obtain a significant decrease in MPIW values on test set through *recalibration*.

4.4 Tube loss based deep probabilistic forecasting models

We have briefly detailed the probabilistic forecasting setup, its related literature and methods in the Section 3.3 of this paper. Now, we extend the Tube loss idea for probabilistic forecasting tasks in deep learning framework.

Given the time-series data $\{y_t, t = 1, 2, \dots, m\}$, lag window $p \leq m$ and target calibration t , the Tube loss based deep probabilistic forecasting models simultaneously obtain the bound of PI by solving the problem

$$\min_{(\mu_1, \mu_2)} \sum_{i=p}^{m-1} \rho_t^r(x_{i+1}, \mu_1(z_i), \mu_2(z_i)) + \delta \sum_{i=p}^{t-1} (|\mu_1(z_i) - \mu_2(z_i)|) \quad (25)$$

where, $\mu_1(z_i)$ and $\mu_2(z_i)$ correspond to the two nodes of the output layer of used deep auto-regressive network such as GRU, LSTM or TCN.

Compared to the quantile-based deep forecasting models (discussed in Section 3.3), Tube loss-based deep forecasting models offer two direct advantages. First, they simplify the probabilistic forecasting process by estimating the bounds of the PI by training a single deep neural architecture, eliminating the need to train multiple models. Second, they are capable of producing narrower PI as they minimize the width of the PI in its optimization problem explicitly. Our empirical results shows that the Tube loss-based models achieve approximately 50% reduction in training time relative to their quantile-based counterparts, while also improves the MPIW values of obtained PI through *recalibration*.

4.5 Tube Loss vs. Existing PI Methods: A Comparative Analysis

In Table 1, we design the desirable criteria of an ideal PI method and compare the existing PI methods like Quantile, LUBE and QD based PI method along with the Tube loss based PI estimation method. We detail the criteria of Table 1 as follows.

- (i) Asymptotic guarantees :- The pinball loss function provides asymptotic guarantees for quantile estimation; therefore, a pair of quantile functions obtained by minimizing corresponding pinball losses can be used to construct PI that asymptotically achieve the desired coverage level. Also, the Tube loss model solves a single problem and provides the asymptotical guarantees for target coverage. Unlike the Quantile and Tube loss-based models, the LUBE and QD loss-based PI estimation methods lack theoretical guarantees for achieving the desired asymptotic coverage.

	Quantile	LUBE	QD loss	Tube loss
Asymptotic guarantees	✓	×	×	✓
Direct PI estimation	×	✓	✓	✓
PI tube movement	✓	×	×	✓
Gradient descent solution	✓	×	✓	✓
Re-calibration	×	✓	✓	✓
Individual Calibration	×	×	×	×

Table 1: Comparisons of the Quantile , LUBE, QD loss and Tube loss based PI estimation models

- (ii) Direct PI estimation:- Unlike quantile-based PI methods, the LUBE, QD, and Tube loss-based models are direct PI estimation approaches, as they can simultaneously learn both bounds of the PI by training a single model.
- (iii) PI tube movement:- The movement of the PI tube helps capture the dense regions of the data cloud, enabling the model to produce narrower PI , especially in the presence of asymmetric noise. The Quantile based PI models enable the movement of the PI tube by choosing the different positive value of q such that $q + t \leq 1$. Also, the Tube loss models can adjust the PI tube by changing their parameter r . The LUBE and QD loss based models do not facilitate the movement of the PI tube.
- (iv) Gradient descent solution:- The pinball loss and Tube loss both are almost differentiable everywhere (re Lebesgue measure) with non-zero gradients. Therefore, their empirical error can be easily back-propagated through the network using the GD method. The LUBE and QD loss function are nonlinear functions of MPIW and PICP. The gradient of the PICP is always zero as it is a step like function. This makes challenging to use GD for optimizing the LUBE and QD models. However, the QD loss function addresses this issue by approximating PICP with a smooth sigmoid function, thereby enabling effective training of the network using GD.
- (v) Re-calibration:- Unlike Quantile, the QD, LUBE and Tube loss models are direct PI estimation models so they can explicitly minimize the width of the PI tube in their optimization problems with a user defined parameter. This allows the models to be *re-calibrated* for lower MPIW values when the empirical coverage on the validation set significantly exceeds the target level t .
- (vi) Individual Calibration : - For given target calibration t , the individual calibration requires that the estimated PI $[\hat{\mu}_1(x), \hat{\mu}_2(x)]$ should contain at least t fraction of y values for each input x . The ideal PI should ensure the individual calibration but, existing PI models in the literature do not guarantee this kind of calibration at the individual level.

4.6 Tube Loss: Extension to the Conformal Regression

The Tube loss methodology can be easily extended to the conformal regression setting for finite sample test set coverage guarantee in distribution-free setting. For split conformal (CR) estimation, the Tube loss-based method simultaneously learns the bound functions $\hat{F}_{lo}(x)$ and $\hat{F}_{hi}(x)$ by training a single network on the training set I_1 . A high-quality PI is then estimated on the calibration set I_2 by tuning the parameters r and δ , if necessary, using I_2 itself. The non-conformity scores E_i , defined in (15), are computed, and the standard conformal prediction step described in (16) is subsequently applied to obtain the prediction set $C(x_{m+1})$.

Tube loss CR method reduces the complexity of the CQR method by simultaneously obtaining the the bound functions $\hat{F}_{lo}(x)$ and $\hat{F}_{hi}(x)$. This advantage becomes increasingly significant as the dataset size grows. Our numerical results demonstrate that the Tube loss-based CR method achieves approximately a 50% reduction in overall computational time compared to the CQR model, without compromising the quality of the prediction set.

5 Experimental Results

In this section, we perform an extensive set of experiments to show the efficacy of the Tube loss function. At first, we compare the Tube loss function for PI estimation task in kernel machine and NN framework with existing PI methods on several artificial and benchmark datasets. Thereafter, we test the performance of Tube loss based deep forecasting models against the recent deep probabilistic forecasting models on several benchmark and wind datasets. Also, we show the advantages of the Tube loss CR model against the popular CQR model by on various benchmark datasets.

For comparing two PI estimation methods, say, A and B we follow this rule: A is better than B (i) if $PICP(A) \geq t$ and $PICP(B) < t$, or (ii) if $\min\{PICP(A), PICP(B)\} \geq t$ and $MPIW(A) < MPIW(B)$. Furthermore, in experiments with synthetic data, the data generated from a known distribution, the true quantiles of y given x are known for all values of x , and thus, the true PI. In such cases, the performance of a PI estimation method is measured by the deviation between the estimated PI, say $[\hat{\mu}_1(x), \hat{\mu}_2(x)]$ and the true PI, say $[\mu_1(x), \mu_2(x)]$. It is measured using the sum of the mean squared error (SMSE) given by $\frac{1}{m} \sum_{i=1}^m (\hat{\mu}_1(x_i) - \mu_1(x_i))^2 + \frac{1}{m} \sum_{i=1}^m (\hat{\mu}_2(x_i) - \mu_2(x_i))^2$.

5.1 Tube loss performance in kernel machine

Let us generate two synthetic datasets, say, **A** and **B**. The data are $\{(x_i, y_i), i = 1, 2, \dots, 1500\}$, where x_i is generated from a uniform distribution between 0 and 1 ($U(0, 1)$) and y_i , using the relation

$$y_i = \frac{\sin x_i}{x_i} + \epsilon_i, \quad (26)$$

where, ϵ_i is a random noise. For dataset **A**, ϵ_i is generated from $\mathcal{N}(0, 0.8)$, a symmetric distribution, and for data set **B** from $\chi^2(3)$, a positively skewed distribution. We train the model using 500 data points and the rest we use for testing. For the estimation of the linear PI tube, we use a linear kernel. For the estimation of the nonlinear PI tube, we use the RBF kernel of the form $k(x_1, x_2) = e^{-\gamma \|(x_1 - x_2)\|^2}$, where γ is a parameter.

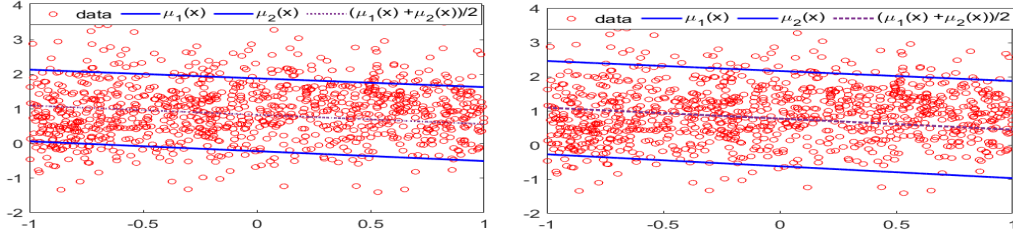


Figure 4: Tube loss based SVPI estimation for (a) $t = 0.8$ and (b) $t = 0.9$.

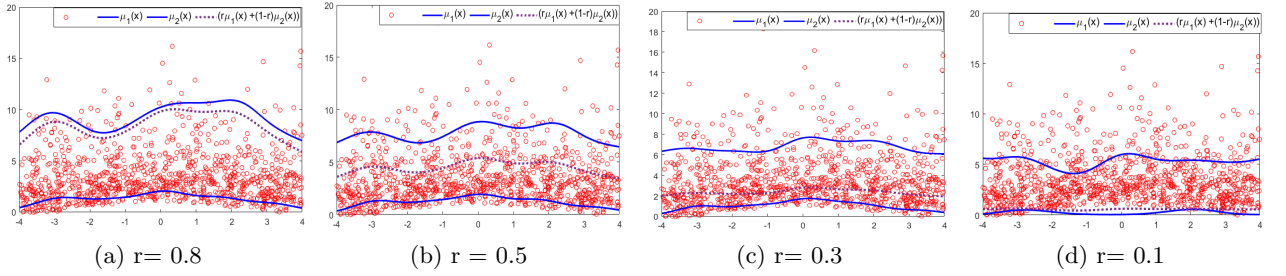


Figure 5: Location of PI tube changes with r values in Tube loss based kernel machine.

For dataset **A**, we obtain PIs with nominal confidence levels $t = 0.8$ and $t = 0.9$ using the Tube loss function with $r = 0.5$ and $\delta = 0$. The PICP and the MPIW of the resulting PI in the test data set corresponding to $t = 0.8$ ($t = 0.9$) are found to be 0.799 (0.909) and 2.10 (2.78), respectively. Figure (4) shows the estimated PI on test set with target $t = 0.8$ and $t = 0.9$.

For dataset **B**, we estimate the PI for $t = 0.8$ with RBF kernel. In Figure 5 (b), the Tube loss based kernel machine with $r = 0.5$ and $\delta = 0$ leads to a PI with PICP 0.79 and MPIW 6.47. Since the noises in the data are generated from a positively skewed distribution, the estimated PI with $r = 0.5$ fails to capture the denser regions of y values across different

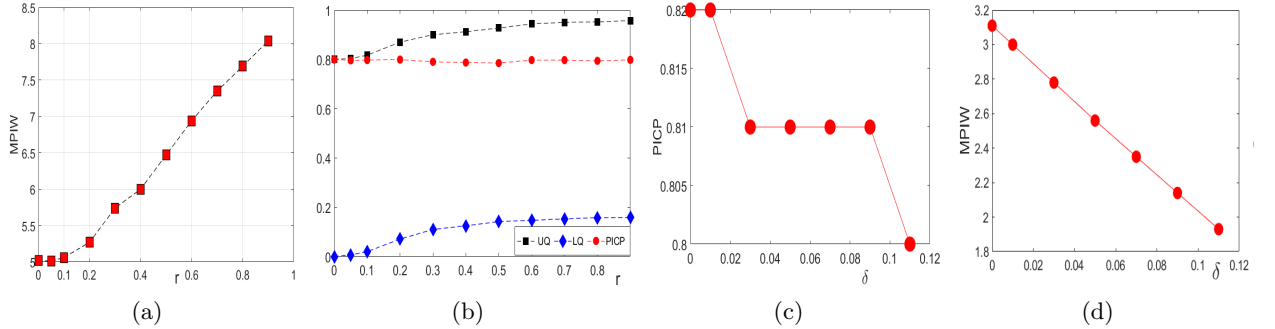


Figure 6: Plot of (a) r against MPIW, (b) PICP, UQ and LQ for dataset **B**. Plot of (c) δ against PICP, (d) δ against MPIW on Servo dataset.

	Model	$(q+t,q)/(r,\delta)$	PICP	MPIW	Time (s)
A	Q Ker M	(0.95,0.15)	0.78 ± 0.017	2.088 ± 0.109	219.38
	Q Ker M	(0.90,0.10)	0.78 ± 0.019	2.002 ± 0.068	221.72
	Q Ker M	(0.85,0.05)	0.79 ± 0.025	2.151 ± 0.078	217.38
	T Ker M	(0.6,0)	0.80 ± 0.012	2.165 ± 0.068	56.93
B	T Ker M	(0.5,0)	0.80 ± 0.018	2.156 ± 0.069	61.50
	Q Ker M	(0.90,30)	0.59 ± 0.032	4.6609 ± 0.153	138.05
	Q Kerl M	(0.95,0.35)	0.58 ± 0.023	5.5369 ± 0.272	146.60
	Q Ker M	(0.80,20)	0.59 ± 0.027	3.6196 ± 0.143	146.41
	T Ker M	(0.3,0)	0.60 ± 0.032	3.495 ± 0.168	39.07
	T Ker M	(0.2,0)	0.601 ± 0.028	3.174 ± 0.165	41.55

Table 2: Quantile based Kernel Machine (Q ker M) and Tube loss based kernel Machine (T ker M) on dataset **A** and **B**. Q kernel M involves parameters $(q+t,q)$ and T kernel M involves (r, δ) .

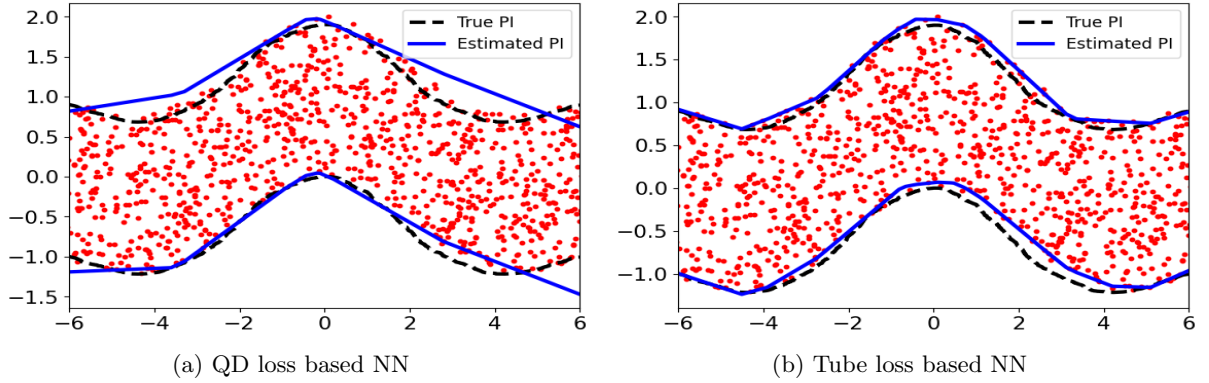


Figure 7: Comparison of Tube loss and QD loss function based NNs

x values, and thus, leading to a large MPIW. Figure 5 (a) indicates that to capture denser regions, the estimated PI tube should be shifted downward. Figures 4(a), 4(c) and 4(d) show the PIs obtained by the tube loss-based kernel machine for $r = 0.8, 0.3$ and 0.1 . The estimated PI tube moves downward with decrease in values of r , thus, capturing denser regions and leading to lowering of MPIW. Figure 6 (a) and (b) show the plots of MPIW, PICP, LQ, and UQ against r . The LQ and UQ denote the fractions of y_i values lying below the upper and the lower bound of our estimated PI tube, respectively. Clearly, the LQ and UQ decrease with the decrease in r leading to a downward movement of the PI tube, and thus, lowering MPIW without changing PICP. The MPIW improves significantly with the decrease in the values of r . In fact, MPIW improves by 21.80%, if we decrease the r from 0.5 to 0.1.

It is worth mentioning here, for data set **A** where the noises are generated by a symmetric distribution, the default choice $r = 0.5$ leads to HQ PI. On the other hand, for the data set **B**, when the noise distribution is positively skewed, the lower value of r leads to HQ PI.

Finally, for both datasets, we compare the performances of PIs using quantile based estimation method and Tube loss based estimation method in kernel machines by replicating

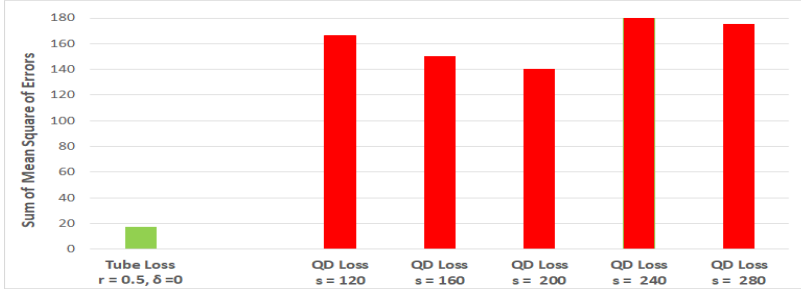


Figure 8: Tube loss based NN approximates true PI better than QD loss.

each experiment 10 times to capture the sampling variation in PICP and MPIW. For dataset **A** (**B**), we run these experiments for nominal confidence level $t = 0.8$ ($t = 0.6$). Notice that for quantile based estimation, the choice of parameter q and for Tube loss-based estimation, the choice of parameters r and δ are crucial for generating HQ interval. Table 1 shows that Tube loss-based method significantly improves the overall training complexity of the PI estimation task. Additionally, it achieves the nominal confidence level consistently, whereas the quantile-based method slightly falls short. Further, as expected for symmetric noises, the Tube loss with $(r = 0.5, \delta = 0)$ yields best PI for dataset **A**. For dataset **B**, on the other hand, we note that MPIW values of the estimated PI can be significantly improved by lowering the value of r . This is expected as the noises are generated from a positively skewed distribution.

Re-calibration effect of parameter δ : As stated above, an appropriate choice of the parameter δ in the Tube loss based kernel machine may lead to the reduction of MPIW on the test set. Let us consider the popular Servo (167×5) Karl Ulrich (2016) data set. A randomly chosen subset comprising 10% of the data points is chosen as the test set. The remaining data points are trained with a 10-fold cross-validation method for obtaining a PI with confidence level $t = 0.8$ considering $r = 0.5$ and $\delta = 0$. The mean PICP reported on the validation set is 0.82. Since the observed PICP is significantly larger than the target confidence $t = 0.8$ on the validation set, therefore, there is a scope to obtain lesser MPIW on the test set by increasing the value of δ . We increase the value of δ till the observed PICP on the validation set decreases to the target $t = 0.8$, shown in Figure 6 (c). It causes about 44% improvement in MPIW in the test set as shown in Figure 6 (d) while maintaining the required coverage.

5.2 Tube Loss performance in Neural Network

In the NN framework Pearce et al. (2018) show that the PI obtained by QD loss performs slightly better than that obtained by LUBE Khosravi et al. (2011a). Also, they observe that the QD method performs far better than the MVE method Nix and Weigend (1994) on benchmark datasets.

Here, we perform a simple experiment to show that the Tube loss based PI outperforms the QD based PI in terms of SMSE, a local measure of smoothness and tightness introduced at the outset of Section 3. For this, we generate 1000 data points (x_i, y_i) using the regression

model,

$$y_i = \frac{\sin(x_i)}{x_i} + \epsilon_i, \quad (27)$$

where x_i is $U(-2\pi, 2\pi)$ and ϵ_i is from $U(-1, 1)$.

We train the tube Loss-based NN model and the QD loss-based NN model to obtain a PI with nominal confidence level 0.95. After tuning, we fix the NN model, containing 100 neurons in the hidden layer with 'RELU' activation function and two neurons in the output layer. 'Adam' optimizer is used for training the NNs. Figure 7 (a) shows the PI obtained by the QD loss and Figure 7 (b) the PI using Tube loss with $r = 0.5$ (Figure 8 b) along with the true PI. Clearly the PI generated by the Tube loss is smoother and tighter compared to that generated by the QD loss. The true PI is computed by obtaining 97.5% and 2.5% quantiles of the conditional distribution of $y|x$ for different values of x .

The observed (PICP, MPIW) for Tube loss and QD loss are (0.95, 1.78) and (0.98, 2.17), respectively. For QD loss, the tuning of the soften parameter s is important but, is a tedious task. We tune parameters s and λ of QD loss to arrive at the choice $s = 200$ and $\lambda = 0.1$. We then compute the SMSEs of the PIs. Figure 8 presents the SMSE comparison of tube loss with QD loss for different values of softening parameter s . Evidently, the performance of the QD loss based PI is sensitive to the choice of s , and thus, on the quality of approximation of the step function by the sigmoidal functions.

Benchmark Datasets:- Here, we consider six open-access data sets, that are commonly considered for comparison in recent UQ literature including Pearce et al. (2018); Chung et al. (2021). Following the experimental setup of Pearce et al. (2018), we compare the performance of the QD loss-based Ensemble (QD-Ens) NN with that of the Tube loss-based Ensemble (Tube-Ens) NN by considering the five NNs per ensemble. The NN models are used to generate 95% PI. (Details of the experiment, its set up and the parameter tuning are provided in Appendix C). Table 3 shows that Tube loss PIs achieve the nominal confidence level of 0.95 consistently with lower MPIW values and outperform the QD loss PIs across all six datasets.

Clearly, Tube loss based PIs outperform QD-Ens based PIs. Some of the reasons are: Tube loss avoids approximations for enabling the use of GD method, asymptotically guarantees nominal confidence level and facilitates movement of the PI bounds by adjusting the tuning parameter r .

Dataset	PICP		MPIW		Better
	QD loss	Tube _{loss}	QD loss	Tube _{loss}	
Boston	0.92 ± 0.01	0.95 ± 0.01	1.16 ± 0.02	1.12 ± 0.04	✓
kin8NM	0.96 ± 0.00	0.95 ± 0.00	1.25 ± 0.01	1.10 ± 0.01	✓
Energy	0.97 ± 0.01	0.95 ± 0.03	0.47 ± 0.01	0.36 ± 0.05	✓
Concrete	0.94 ± 0.01	0.95 ± 0.02	1.09 ± 0.01	1.22 ± 0.06	✓
Naval	0.98 ± 0.00	0.95 ± 0.01	0.28 ± 0.01	0.24 ± 0.03	✓
Wine	0.92 ± 0.01	0.95 ± 0.01	2.33 ± 0.02	2.80 ± 0.08	✓

Table 3: PI quality metric on real-world benchmark datasets.

5.3 Probabilistic Forecasting with Tube loss based Deep Networks

We now assess and compare the performance of the Tube loss based probabilistic forecasting using different deep NN architectures, viz. LSTM, GRU and TCN with existing probabilistic forecasting algorithms.

At first, we consider the six popular benchmark time-series data sets viz., Electric (BP and Ember. (2016)), Sunspots (SIDC and Quandl.), SWH (NDBC), Temperature (machine-learningmastery.com), Female Birth (datamarket.com) and Beer Production (Australian (1996)). For probabilistic forecasts on these datasets, we compare the performance of the Tube loss based LSTM (T-LSTM) with that of the Quantile based LSTM (Q-LSTM). We use 70% of the data points for training and rest for testing. From each of the training sets, 10% of the observations are used for validation.

Dataset	PICP		MPIW		Training Time (SEC)		Improvement in Time(s)	Improvement in MPIW	Better
	Q-LSTM	T- LSTM	Q-LSTM	T-LSTM	Q-LSTM	T-LSTM			
Electric	0.95	0.95	18.23	17.02	145	58	60 %	6.60 %	✓
Sunspots	0.93	0.95	121.09	113.98	839	442	47 %	5.87 %	✓
SWH	0.96	0.96	0.52	0.35	5119	2733	46 %	32.69%	✓
Temperature	0.95	0.94	24.82	15.56	1135	447	60 %	37.30%	✓
Female Birth	0.95	0.96	28.20	28.09	118	43	63 %	0.40%	✓
Beer Production	0.94	0.95	134.8	42.91	132.8	89.6	33 %	68.17%	✓

Table 4: Comparison of Quantile based LSTM (Q-LSTM) and Tube loss based LSTM (T-LSTM) on real-world time-series datasets

Since these datasets were used by other researchers, for each dataset, we tune and fix LSTM hidden layer structure, drop out layer and window size based on information available in the literature. We then obtain the PI using the Tube loss function, and also using quantiles. The nominal confidence level considered is 0.95. In Table 4, the PICP, MPIW and training time in seconds are reported for Q-LSTM and T-LSTM. Clearly, the T-LSTM based PIs outperform Q-LSTM based PIs in five out of 6 datasets. Also, re-calibration of the Tube loss leads to further reduction of MPIW. But, the main advantage of T-LSTM over Q-LSTM is significant improvement in the MPIW values and training time. As stated above, Q-LSTM needs to be trained twice whereas T-LSTM requires training only once.

The probabilistic forecasts for each of the data sets considered in Table 3 are presented in Figure 11 of Appendix C. The details of the LSTM architectures, and the values of the tuning parameters used for obtaining the probabilistic forecasts for each data set are presented in Table 9 of Appendix C.

In a distribution-free setting, quantile-based deep learning models are the most popular choice for probabilistic forecasting. However, we also need to compare the performance of the Tube loss based probabilistic forecasting with that of the deep learning models trained with the QD loss function (Pearce et al. (2018)) . A significant practical challenge in training deep learning models with the QD loss function Pearce et al. (2018) is the frequent occurrence of NaN losses during computation. However, the extended Quality Driven (QD^+) loss function (Salem et al. (2020)) solves this problem up to some extent. Consequently, we have implemented the QD^+ loss function based deep forecasting models for obtaining the probabilistic forecast. We tune the parameter values of QD^+ loss function based LSTM

well and compare its performance with the Tube loss based LSTM model on time-series benchmark dataset at Table 5. Unlike, the Quantile and Tube loss based LSTM models, the QD+ loss function based LSTM model fails to obtain the consistent performance. Out of six datasets, it fails to obtain the target coverage on three datasets. In case of Sunspots and Temperature datasets, the QD+ loss function based LSTM obtains very poor performance. Additionally, across all datasets, the Tube loss LSTM models outperform the QD+ loss LSTM models.

Dataset	PICP		MPIW		Improvement in MPIW	Better
	QD ⁺ -LSTM	T- LSTM	QD ⁺ -LSTM	T-LSTM		
Electric	0.96	0.95	54.63	17.02	68.84 %	✓
Sunspots	0.43	0.95	24.06	113.98	NA	✓
SWH	0.96	0.96	0.36	0.35	2.78%	✓
Female Birth	0.94	0.96	38.98	28.09	27.94%	✓
Temperature	0.79	0.95	5.94	15.56	73.13 %	✓
Beer Production	0.96	0.95	159.71	42.91	NA	✓

Table 5: Comparison of Extended Quality Driven loss based LSTM (QD⁺ LSTM) and Tube loss based LSTM (T-LSTM) on real-world time-series datasets

5.4 Probabilistic forecasting of wind speed with Tube loss

Due to the unpredictable nature of wind, it is very difficult to obtain the accurate forecast of wind speed. Probabilistic forecasting of wind speed is crucial for effective decision-making in the wind power industry. It helps evaluate potential risks and outcomes, supporting better planning for grid operations and more reliable participation in the electricity market. We systematically details the different steps involved in our probabilistic forecasting experiments as follows.

- (i) **Dataset Collection:-** We selected two datasets collected from two different locations: Jaisalmer and San Francisco. The Jaisalmer dataset contains hourly wind speed measurements at a height of 120 meters for 8,760 hours, while the San Francisco dataset includes 26,304 hourly observations at the same height. To demonstrate the effectiveness of the Tube loss methodology, we applied it using three popular deep auto-regressive models: LSTM, GRU, and TCN.
- (ii) **Details of the experiment-** The wind speed time series dataset was divided by reserving the last 30% of observations as the test set, while the final 10% of the remaining training data was used for validation. The target coverage level for the probabilistic forecasting task was set to $t = 0.95$.
- (iii) **Baseline Methods:-** Quantile regression using the pinball loss function is one of the most widely adopted approaches for probabilistic wind speed forecasting. Several studies have explored neural and deep learning models based on this technique, including works such as (Heng et al. (2022), Cui et al. (2017), Hu et al. (2020b), Wan et al. (2016), Yu et al. (2021), Zhu et al. (2022), Cui et al. (2022)), and (Zhu and

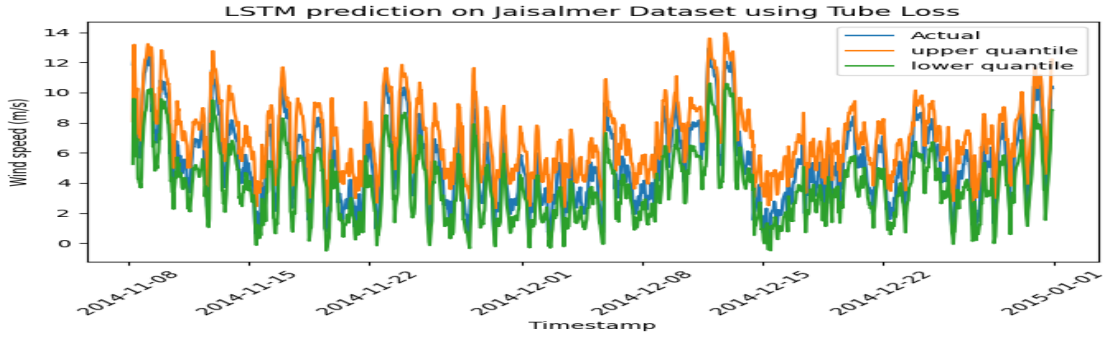
Rank	Model	PICP	MPIW	MPIW/PICP
1	GRU + Tube	0.9550	3.392	3.55
2	TCN + Tube	0.9581	3.453	3.60
3	TCN + QD ⁺	0.9589	3.511	3.66
4	LSTM + Tube	0.9589	3.697	3.86
5	GRU + QD ⁺	0.9666	3.966	4.10
6	TCN + Quantile	0.9674	4.094	4.23
7	LSTM + QD ⁺	0.9689	4.470	4.61
8	MDN	0.955	4.626	4.84
9	LSTM + Quantile	0.979	4.937	5.04
10	GRU + Quantile	0.9891	5.365	5.43
11	Deep AR	0.9969	6.3553	6.38
12	Time GPT	0.9417	10.608	11.27

Table 6: Ranking of different deep probabilistic forecasting methods on Jaisalmer Dataset.

Rank	Model	PICP	MPIW	MPIW/PICP
1	TCN + Tube	0.9543	4.560	4.78
2	LSTM + Tube	0.9561	4.627	4.84
3	GRU + Tube	0.9507	4.857	5.11
4	GRU + Quantile	0.951	4.955	5.21
5	LSTM + Quantile	0.9594	5.407	5.64
6	TCN + QD ⁺	0.9505	5.490	5.78
7	LSTM + QD ⁺	0.9734	6.043	6.21
8	Deep AR	0.9855	6.2023	6.29
9	GRU + QD ⁺	0.9724	6.309	6.49
10	MDN	0.949	4.620	4.87
11	TCN + Quantile	0.9428	4.908	5.21
12	TimeGPT	0.9357	11.235	12.00

Table 7: Ranking of different deep probabilistic forecasting methods on Jaisalmer Dataset.

He (2024)). Additionally, QD loss-based deep architectures have been used for wind forecasting in (Saeed et al. (2024)) and (Hu et al. (2020a)). Accordingly, we use LSTM, GRU, and TCN architectures trained with pinball loss functions as baseline methods



(a)

Figure 9: Probabilistic forecast of the Tube loss based LSTM on Jaisalmer wind dataset.

in our experiments. For avoiding the occurrence of NaN losses during the computation, we use the QD^+ loss function in place of QD loss function in LSTM, GRU, and TCN architectures for obtaining the probabilistic forecast of wind speed. Recently, the DeepAR model (Salinas et al. (2020)) has gained popularity for probabilistic forecasting and has been applied in various time series applications, including wind power forecasting (Arora et al. (2022)). Moreover, several recent studies, such as (Yang et al. (2021), Zhang et al. (2020)), and (Men et al. (2016)), demonstrate the effectiveness of Mixture Density Networks (MDN) in wind forecasting. Therefore, we also include DeepAR and MDN as baseline models in our evaluation. In addition, we incorporate the pre-trained Time-GPT model (Garza et al. (2023)), a foundation model for time series forecasting, as another baseline for comparison.

- (iv) **Numerical Results:-** We have trained different deep forecasting architectures such as GRU, LSTM and TCN with the Tube loss function on Jaisalmer and San Francisco datasets and compared their performance with existing baseline methods for probabilistic forecast at Table 6 and 7 respectively. In these tables, the probabilistic forecasting models are ranked according to the comparison rules outlined at the beginning of the experimental section.
- (v) **Analysis:-** In Tables 6 and 7, we observe that the Tube loss-based probabilistic forecasting models consistently achieve the target coverage for future wind observations by calibrating narrower PIs. The Tube loss-based deep forecasting models secure top ranks in both tables and outperform recent wind probabilistic forecasting models from the literature. Figure 9 shows the probabilistic forecast obtained by the Tube loss LSTM model on Jaisalmer dataset.

5.5 Tube loss performance in Conformal Regression

At last, we compare the Tube loss based Conformal Regression (TCR) model with the CQR model (Romano et al. (2019)) to show the efficacy of the Tube loss approach over the quantile approach in conformal regression setting. To conduct this evaluation, we use popular benchmark datasets and randomly split each into training, calibration, and test sets in a ratio of 3:1:1, repeated across ten different trials. We test the performance of the CQR and TCR in each trail and report the mean of PICP and MPIW in Table 8 by setting the target calibration $t = 0.9$. We also record the number of trials in which a given CR model fails to achieve the target calibration level of $t = 0.9$, denoted as “Error” and report these values for both the CQR and TCR models in Table 8 for the comparison. Across 90 trials conducted on the 9 benchmark datasets listed in Table 8, the CQR model failed to achieve the target calibration on the test set in 29 cases, while the TCR model failed in 21 cases. The TCR model achieves a significant reduction in total training time compared to the CQR model, with an improvement of approximately 47%. This is primarily because TCR estimates both quantile bounds simultaneously by training a single network.

6 Future Work

The Tube loss method provides an effective approach for simultaneously estimating a pair of quantile functions. As such, it holds strong potential to replace traditional quantile-based

Dataset	PICP		Error		MPIW		Time (s)	
	CQR	TCQR	CQR	TCQR	CQR	TCQR	CQR	TCQR
Concrete	0.90 ± 0.04	0.91 ± 0.03	2	3	17.11 ± 1.76	19.89 ± 1.46	34.04 ± 2.66	17.32 ± 1.99
Bike	0.90 ± 0.01	0.90 ± 0.01	3	3	192.51 ± 43.23	171.77 ± 9.12	74.36 ± 7.05	40.21 ± 4.31
Star	0.90 ± 0.02	0.90 ± 0.02	3	3	1022.19 ± 40.99	982.83 ± 43.13	32.06 ± 2.36	16.28 ± 1.16
Community	0.90 ± 0.02	0.91 ± 0.02	5	1	0.43 ± 0.02	0.47 ± 0.02	17.30 ± 3.61	9.01 ± 0.18
Facebook	0.91 ± 0.01	0.90 ± 0.00	0	1	18.51 ± 4.46	17.78 ± 1.63	182.81 ± 5.48	99.35 ± 3.53
Boston Housing	0.89 ± 0.03	0.92 ± 0.03	6	2	9.38 ± 0.73	13.12 ± 3.70	4.73 ± 0.06	2.66 ± 0.07
Naval	0.90 ± 0.01	0.90 ± 0.01	1	4	0.02 ± 0.00	0.02 ± 0.00	83.10 ± 6.92	46.70 ± 4.28
Yatch Hydro	0.86 ± 0.04	0.90 ± 0.05	7	4	2.37 ± 0.71	2.47 ± 0.56	41.72 ± 8.54	20.39 ± 3.39
Auto MPG	0.92 ± 0.04	0.93 ± 0.04	2	1	10.03 ± 0.94	9.90 ± 1.24	53.21 ± 4.64	28.11 ± 4.18

Table 8: Comparison of the TCR method with CQR method on different benchmark datasets

methods in applications where both lower and upper quantile functions are required to be estimated. The future work requires a detailed theoretical analysis of the Tube loss function, similar to the analysis of the pinball loss function available in the literature.

Like existing methods, the Tube loss approach also does not guarantee the target calibration t locally. A promising direction for future work is to enhance the Tube loss-based networks by incorporating techniques from the literature, such as group batching (Chung et al. (2021)) or orthogonality constraints (Feldman et al. (2021)), to improve their local calibration performance. Additionally, there is a need to develop new non-conformity scores that align with the Tube loss methodology to improve the prediction sets in the conformal regression setting.

In most applications related to the text processing, the target variable is multidimensional. An interesting problem is to consider extension of the proposed Tube loss approach for multidimensional target variable in PI estimation and conformal regression settings. Also, it would be interesting to use the Tube loss functions with different auto-regressive neural architectures for obtaining the high quality probabilistic forecast in different domains of applications, such as solar irradiance, cryptocurrency prices, exchange rates, stock prices, ocean wave heights, pollution rates, and weather forecasting, to name a few.

Acknowledgments and Disclosure of Funding

Authors are thankful to Harsh Sawaliya, Kashyap Patel, Aadesh Minz, Asish Joel, Kadia Akshat Hardikumar and Jyaswal Krishil Alpeshbhai for extending their help in conducting the numerical experiments. This work was funded by the Smart Energy Learning Center at DA-IICT, Gandhinagar through Grant no.- CSR-25/BSES/A6-PA/SELIC.

Appendix A. Proof of the Lemma 1

Let us assume that $\#\{y_i | y_i = \mu_2^*\} = k_1$, $\#\{y_i | y_i = r\mu_2^* + (1-r)\mu_1^*\} = k_2$, and $\#\{y_i | y_i = \mu_1^*\} = k_3$, where $\#$ represents the cardinality of a set. In other words, k_1, k_2 and k_3 represent the number of points on the boundary sets. Thus, we obtain $m_1 + k_1 + m_2 + k_2 + m_3 + k_3 + m_4 = m$.

Let us choose, $\delta_1^* \in [0, \epsilon_1)$, $\delta_2^* \in [0, \epsilon_2)$, where ϵ_1 and ϵ_2 are positive real numbers, such that $\epsilon_1 \geq \min_{y_i < \mu_1^*} (|\mu_1^* - y_i|)$, $\epsilon_2 \geq \min_{y_i > \mu_2^*} |(y_i - \mu_2^*)|$, and $r\epsilon_2 + (1-r)\epsilon_1 < \min_{\mu_1^* < y_i < \mu_2^*} |y_i - (r\mu_2^* + (1-r)\mu_1^*)|$, which entails

$$\begin{aligned} \#\{y_i : \mu_2^* < y_i \leq \mu_2^* + \delta_2^*\} &= 0, \quad \#\{y_i : \mu_2^* < y_i \leq \mu_2^* - \delta_2^*\} = 0, \quad \#\{y_i : \mu_1^* < y_i \leq \mu_1^* + \delta_1^*\} = 0, \\ \#\{y_i : \mu_1^* < y_i \leq \mu_1^* - \delta_1^*\} &= 0, \quad \#\{r\mu_2^* + (1-r)\mu_1^* < y_i \leq r(\mu_2^* + \delta_2^*) + (1-r)(\mu_1^* + \delta_1^*)\} = 0, \\ \#\{r\mu_2^* + (1-r)\mu_1^* < y_i \leq r(\mu_2^* - \delta_2^*) + (1-r)(\mu_1^* - \delta_1^*)\} &= 0. \end{aligned}$$

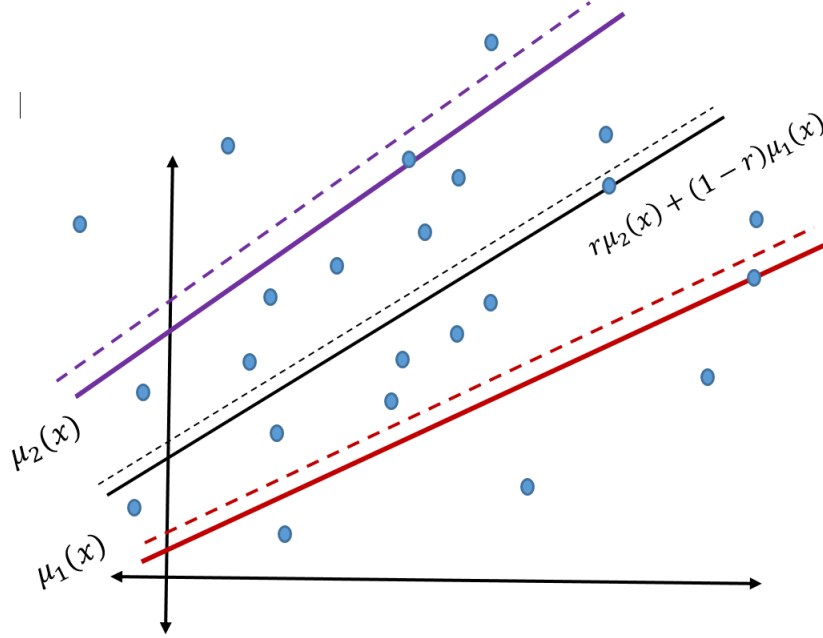


Figure 10:

Given that (μ_1^*, μ_2^*) is an optimal solution, we have $\sum_{i=1}^m \rho_t^r(y_i, \mu_1^* + \delta_1^*, \mu_2^* + \delta_2^*) - \sum_{i=1}^m \rho_t^r(y_i, \mu_1^*, \mu_2^*) \geq 0$. We now evaluate the difference of the sums for each of the following ten sets inducing a partition of \mathbb{R} .

$$\begin{aligned} R_1 &= \{y_i : y_i > \mu_2^* + \delta_2^*\}, R_2 = \{y_i : \mu_2^* < y_i \leq \mu_2^* + \delta_2^*\}, R_3 = \{y_i : y_i = \mu_2^*\}, \\ R_4 &= \{y_i : r(\mu_2^* + \delta_2^*) + (1-r)(\mu_1^* + \delta_1^*) < y_i < \mu_2^*\}, R_5 = \{y_i : r\mu_2^* + (1-r)\mu_1^* < y_i \leq \\ &r(\mu_2^* + \delta_2^*) + (1-r)(\mu_1^* + \delta_1^*)\}, R_6 = \{y_i : y_i = r\mu_2^* + (1-r)\mu_1^*\}, R_7 = \{y_i : \mu_1^* + \delta_1^* < \\ &y_i < r\mu_2^* + (1-r)\mu_1^*\}, R_8 = \{y_i : \mu_1^* < y_i \leq \mu_1^* + \delta_1^*\}, R_9 = \{y_i : y_i = \mu_1^*\}, R_{10} = \{y_i : y_i < \mu_1^*\}. \end{aligned}$$

Denote the difference $\sum_{y_i \in R_i} \rho_t^r(y_i, \mu_1^* + \delta_1^*, \mu_2^* + \delta_2^*) - \sum_{y_i \in R_i} \rho_t^r(y_i, \mu_1^*, \mu_2^*)$ by Δ_i . The simple calculation leads to the following values of $\Delta_i, i = 1, 2, \dots, 10$: $\Delta_1 = -tm_1\delta_2^*, \Delta_2 =$

$$0, \Delta_3 = (1-t)k_1\delta_2^*, \Delta_4 = (1-t)m_2\delta_2^*, \Delta_5 = 0, \Delta_6 = k_2(1-t)(\delta_1^* + (2-r)\mu_1^* - (1-r)\mu_2^*), \Delta_7 = -(1-t)m_3\delta_1^*, \Delta_8 = 0, \Delta_9 = tk_3\delta_1^*, \Delta_{10} = tm_4\delta_1^*.$$

Thus, we obtain

$$\sum_{i=1}^m \rho_t^r(y_i, \mu_1^* + \delta_1^*, \mu_2^* + \delta_2^*) - \sum_{i=1}^m \rho_t^r(y_i, \mu_1^*, \mu_2^*) = -tm_1\delta_2^* + (1-t)k_1\delta_2^* + (1-t)m_2\delta_2^* + (1-t)k_2(\delta_1^* + (2-r)\mu_1^* - (1-r)\mu_2^*) - (1-t)m_3\delta_1^* + tk_3\delta_1^* + tm_4\delta_1^* \geq 0. \quad (28)$$

If we assume $\delta_1^* = 0$ and $\delta_2^* > 0$, the above inequality entails

$$\frac{1-t}{t} \geq \frac{m_1\delta_2^*}{m_2\delta_2^* + k_1\delta_2^* + k_2((2-r)\mu_1^* - (1-r)\mu_2^*)}.$$

Given that y_i 's are the realizations of a continuous random variable with no discrete probability mass, $k_1/m, k_2/m \rightarrow 0$ with probability 1 as $m \rightarrow \infty$. Thus, as $m \rightarrow \infty$, with probability 1,

$$\frac{m_1}{m_2} \leq \frac{1-t}{t}. \quad (29)$$

Arguing on a similar line, if we consider $\delta_2^* = 0$ and $\delta_1^* > 0$ in 28, then we have the following inequality

$$\frac{(k_3 + m_4)\delta_1^*}{m_3\delta_1^* - k_2(\delta_1^* + (2-r)\mu_1^* - (1-r)\mu_2^*)} \geq \frac{1-t}{t}$$

As $m \rightarrow \infty$, we can state that the following inequality holds with probability 1,

$$\frac{m_4}{m_3} \geq \frac{1-t}{t}. \quad (30)$$

Again, starting with (μ_1^*, μ_2^*) as an optimal solution, we have $\sum_{i=1}^m \rho_t^r(y_i, \mu_1^* - \delta_1^*, \mu_2^* - \delta_2^*) - \sum_{i=1}^m \rho_t^r(y_i, \mu_1^*, \mu_2^*) \geq 0$. For computing this, let us evaluate the difference of the sums for each of the following ten sets inducing a partition of \mathbb{R} .

$$R'_1 = \{y_i : y_i > \mu_2^*\}, R'_2 = \{y_i : y_i = \mu_2^*\}, R'_3 = \{y_i : \mu_2^* - \delta_2^* \leq y_i < \mu_2^*\}, R'_4 = \{y_i : r\mu_2^* + (1-r)\mu_1^* < y_i < \mu_2^* - \delta_2^*\}, R'_5 = \{y_i : y_i = r(\mu_2^*) + (1-r)\mu_1^*\}, R'_6 = \{y_i : r(\mu_2^* - \delta_2^*) + (1-r)(\mu_1^* - \delta_1^*) \leq y_i < r\mu_2^* + (1-r)\mu_1^*\}, R'_7 = \{\mu_1^* < y_i < r(\mu_2^* - \delta_2^*) + (1-r)(\mu_1^* - \delta_1^*)\}, R'_8 = \{y_i : y_i = \mu_1^*\}, R'_9 = \{y_i : \mu_1^* < y_i \leq \mu_1^* - \delta_1^*\}, R'_{10} = \{y_i : y_i < \mu_1^* - \delta_1^*\}.$$

Denoting $\sum_{y_i \in R_i} \rho_t^r(y_i, \mu_1^* - \delta_1^*, \mu_2^* - \delta_2^*) - \sum_{y_i \in R_i} \rho_t^r(y_i, \mu_1^*, \mu_2^*)$ by Δ'_i we obtain the following values of $\Delta'_i, i = 1, 2, \dots, 10$: $\Delta'_1 = tm_1\delta_2^*, \Delta'_2 = -(1-t)k_1\delta_2^*, \Delta'_3 = 0, \Delta'_4 = -(1-t)m_2\delta_2^*, \Delta'_5 = -(1-t)k_2\delta_2^*, \Delta'_6 = 0, \Delta'_7 = (1-t)m_3\delta_1^*, \Delta'_8 = (1-t)k_3\delta_1^*, \Delta'_9 = 0, \Delta'_{10} = -tm_4\delta_1^*$.

Thus, we obtain

$$\sum_{i=1}^m \rho_t^r(y_i, \mu_1^* + \delta_1^*, \mu_2^* + \delta_2^*) - \sum_{i=1}^m \rho_t^r(y_i, \mu_1^*, \mu_2^*) = tm_1\delta_2^* - (1-t)k_1\delta_2^* - (1-t)m_2\delta_2^* - (1-t)k_2\delta_2^* + (1-t)m_3\delta_1^* + (1-t)k_3\delta_1^* - tm_4\delta_1^* \geq 0. \quad (31)$$

Now, if we assume $\delta_1^* = 0$ and $\delta_2^* > 0$ in (31), then we obtain,

$$\frac{m_1}{k_1 + m_2 + k_2} \geq \frac{1-t}{t},$$

which entails

$$\frac{m_1}{m_2} \geq \frac{1-t}{t}, \quad (32)$$

as $m \rightarrow \infty$ with probability 1.

Similarly, considering $\delta_2^* = 0$ and $\delta_1^* > 0$ in (31), we obtain as $m \rightarrow \infty$,

$$\frac{m_4}{m_3} \leq \frac{1-t}{t}, \quad (33)$$

holds with probability 1.

Thus, (29) and (32) imply that as $m \rightarrow \infty$

$$\frac{m_1}{m_2} = \frac{1-t}{t} \quad (34)$$

holds with probability 1.

Similarly, combining (30) and (32), we obtain as $m \rightarrow \infty$,

$$\frac{m_4}{m_3} = \frac{1-t}{t} \quad (35)$$

holds with probability 1.

Thus, combining 34 and 35, we obtain, as $m \rightarrow \infty$,

$$\frac{m_1 + m_4}{m_2 + m_3} = \frac{1-t}{t} \quad (36)$$

holds with probability 1.

Appendix B. Gradient Descent method for Tube loss based kernel machine

The Tube loss based kernel machine considers the problem

$$\begin{aligned} \min_{(\alpha, \beta, b_1, b_2)} J_2(\alpha, \beta, b_1, b_2) &= \frac{\lambda}{2} (\alpha^T \alpha + \beta^T \beta) + \sum_{i=1}^m \rho_t^r(y_i, (K(A^T, x_i)\alpha + b_1), (K(A^T, x_i)\beta + b_2)) \\ &\quad + \delta \sum_{i=1}^m |(K(A^T, x_i)(\alpha - \beta) + (b_1 - b_2))|, \end{aligned} \quad (37)$$

where ρ_t^r is the Tube loss function as given in (20) with the parameter r .

For a given point (x_i, y_i) , let us compute the gradient of $\rho_i^r(y_i, (K(A^T, x_i)\alpha + b_1), (K(A^T, x_i)\beta + b_2))$ first. For this, we compute

$$\begin{aligned}
& \frac{\partial \rho_i^r(y_i, (K(A^T, x_i)\alpha + b_1), (K(A^T, x_i)\beta + b_2))}{\partial \alpha} = \\
& \begin{cases} (1-t)K(A, x_i), & \text{if } (K(A^T, x_i)\beta + b_2) < y_i < (K(A^T, x_i)\alpha + b_1) \text{ and } y_i > (K(A^T, x_i)(r\alpha + (1-r)\beta) + (rb_1 + (1-r)b_2)). \\ 0, & \text{if } (K(A^T, x_i)\beta + b_2) < y_i < (K(A^T, x_i)\alpha + b_1) \text{ and } y_i < (K(A^T, x_i)(r\alpha + (1-r)\beta) + (rb_1 + (1-r)b_2)). \\ 0, & \text{if } K(A^T, x_i)\beta + b_2 > y. \\ -tK(A^T, x_i), & \text{if } K(A^T, x_i)\alpha + b_1 < y. \end{cases} \\
& \frac{\partial \rho_i^r(y_i, (K(A^T, x_i)\alpha + b_1), (K(A^T, x_i)\beta + b_2))}{\partial b_1} = \\
& \begin{cases} (1-t), & \text{if } (K(A^T, x_i)\beta + b_2) < y_i < (K(A^T, x_i)\alpha + b_1) \text{ and } y_i > (K(A^T, x_i)(r\alpha + (1-r)\beta) + (rb_1 + (1-r)b_2)). \\ 0, & \text{if } (K(A^T, x_i)\beta + b_2) < y_i < (K(A^T, x_i)\alpha + b_1) \text{ and } y_i < (K(A^T, x_i)(r\alpha + (1-r)\beta) + (rb_1 + (1-r)b_2)). \\ 0, & \text{if } K(A^T, x_i)\beta + b_2 > y. \\ -t, & \text{if } K(A^T, x_i)\alpha + b_1 < y. \end{cases} \\
& \frac{\partial \rho_i^r(y_i, (K(A^T, x_i)\alpha + b_1), (K(A^T, x_i)\beta + b_2))}{\partial \beta} = \\
& \begin{cases} 0, & \text{if } (K(A^T, x_i)\beta + b_2) < y_i < (K(A^T, x_i)\alpha + b_1) \text{ and } y_i > (K(A^T, x_i)(r\alpha + (1-r)\beta) + (rb_1 + (1-r)b_2)). \\ -(1-t)K(A, x_i), & \text{if } (K(A^T, x_i)\beta + b_2) < y_i < (K(A^T, x_i)\alpha + b_1) \text{ and } y_i < (K(A^T, x_i)(r\alpha + (1-r)\beta) + (rb_1 + (1-r)b_2)). \\ tK(A, x_i), & \text{if } K(A^T, x_i)\beta + b_2 > y. \\ 0, & \text{if } K(A^T, x_i)\alpha + b_1 < y. \end{cases} \\
& \frac{\partial \rho_i^r(y_i, (K(A^T, x_i)\alpha + b_1), (K(A^T, x_i)\beta + b_2))}{\partial b_2} = \\
& \begin{cases} 0, & \text{if } (K(A^T, x_i)\beta + b_2) < y_i < (K(A^T, x_i)\alpha + b_1) \text{ and } y_i > (K(A^T, x_i)(r\alpha + (1-r)\beta) + (rb_1 + (1-r)b_2)). \\ -(1-t), & \text{if } (K(A^T, x_i)\beta + b_2) < y_i < (K(A^T, x_i)\alpha + b_1) \text{ and } y_i < (K(A^T, x_i)(r\alpha + (1-r)\beta) + (rb_1 + (1-r)b_2)). \\ t, & \text{if } K(A^T, x_i)\beta + b_2 > y. \\ 0, & \text{if } K(A^T, x_i)\alpha + b_1 < y. \end{cases}
\end{aligned}$$

For data point (x_k, y_k) such that $y_k = K(A^T, x_k)\alpha + b_1$, or $K(A^T, x_k)\beta + b_2$, the unique gradient for Tube loss does not exist and any sub-gradient can be considered for computation. The data point (x_k, y_k) lying exactly upon the surface $r((K(A^T, x_k)\alpha) + b_1) + (1-r)(K(A^T, x_k)\beta + b_2)$ can be ignored.

Now, for given data point (x_i, y_i) , we consider the width of PI tube $\delta|(K(A^T, x_i, y_i)(\alpha - \beta) + (b_1 - b_2))|$ and denote it as $J(\alpha, \beta, b_1, b_2, x_i, y_i)$ and compute

$$\begin{aligned}
& \frac{\partial J(\alpha, \beta, b_1, b_2, x_i)}{\partial \alpha} = \text{sign}((K(A^T, x_i)(\alpha - \beta) + (b_1 - b_2))K(A^T, x_i)) \quad \text{if } (K(A^T, x_i)(\alpha - \beta) + (b_1 - b_2)) \neq 0 \\
& \frac{\partial J(\alpha, \beta, b_1, b_2, x_i)}{\partial b_1} = \text{sign}((K(A^T, x_i)(\alpha - \beta) + (b_1 - b_2))) \quad \text{if } (K(A^T, x_i)(\alpha - \beta) + (b_1 - b_2)) \neq 0 \\
& \frac{\partial J(\alpha, \beta, b_1, b_2, x_i)}{\partial \beta} = -\text{sign}((K(A^T, x_i)(\alpha - \beta) + (b_1 - b_2))K(A^T, x_i)) \quad \text{if } (K(A^T, x_i)(\alpha - \beta) + (b_1 - b_2)) \neq 0 \\
& \frac{\partial J(\alpha, \beta, b_1, b_2, x_i)}{\partial b_2} = -\text{sign}((K(A^T, x_i)(\alpha - \beta) + (b_1 - b_2))) \quad \text{if } (K(A^T, x_i)(\alpha - \beta) + (b_1 - b_2)) \neq 0
\end{aligned}$$

For data point (x_i, y_i) satisfying $(K(A^T, x_i)(\alpha - \beta) + (b_1 - b_2)) = 0$, unique gradient of $J(\alpha, \beta, b_1, b_2, x_i, y_i)$ does not exist and any sub gradient can be considered for computation.

Now, we state gradient descent algorithm for the Tube loss based kernel machine problem.

Algorithm 2:-

Input:- Training Set $T = \{(x_i, y_i) : x_i \in \mathbb{R}^n, y_i \in \mathbb{R}, i = 1, 2, \dots, m\}$, confidence $t \in (0, 1)$
 r, δ, η and tol .

Initialize:- $\alpha^0, \beta^0 \in \mathbb{R}^m$ and $b_1^0, b_2^0 \in \mathbb{R}$.

Repeat

$$\begin{aligned}\beta^{(k+1)} &= \beta^{(k)} - \eta_k \left(\lambda \beta^{(k)} + \sum_{i=1}^m \frac{\partial \rho_t^r(y_i, (K(A^T, x_i)\alpha + b_1), (K(A^T, x_i)\beta + b_2))}{\partial \beta^{(k)}} + \delta \sum_{i=1}^m \frac{\partial J(\alpha, \beta, b_1, b_2, x_i, y_i)}{\partial \beta^{(k)}} \right) \\ b_2^{(k+1)} &= b_2^{(k)} - \eta_k \left(\sum_{i=1}^m \frac{\partial \rho_t^r(y_i, (K(A^T, x_i)\alpha + b_1), (K(A^T, x_i)\beta + b_2))}{\partial b_2^{(k)}} + \delta \sum_{i=1}^m \frac{\partial J(\alpha, \beta, b_1, b_2, x_i, y_i)}{\partial b_2^{(k)}} \right) \\ \alpha^{(k+1)} &= \alpha^{(k)} - \eta_k \left(\lambda \alpha^{(k)} + \sum_{i=1}^m \frac{\partial \rho_t^r(y_i, (K(A^T, x_i)\alpha + b_1), (K(A^T, x_i)\beta + b_2))}{\partial \alpha^{(k)}} + \delta \sum_{i=1}^m \frac{\partial J(\alpha, \beta, b_1, b_2, x_i, y_i)}{\partial \alpha^{(k)}} \right) \\ b_1^{(k+1)} &= b_1^{(k)} - \eta_k \left(\sum_{i=1}^m \frac{\partial \rho_t^r(y_i, (K(A^T, x_i)\alpha + b_1), (K(A^T, x_i)\beta + b_2))}{\partial b_1^{(k)}} + \delta \sum_{i=1}^m \frac{\partial J(\alpha, \beta, b_1, b_2, x_i, y_i)}{\partial b_1^{(k)}} \right)\end{aligned}$$

Until $\left\| \begin{bmatrix} \alpha^{(k+1)} - \alpha^{(k)} \\ b_1^{(k+1)} - b_1^{(k)} \\ \beta^{(k+1)} - \beta^{(k)} \\ b_2^{(k+1)} - b_2^{(k)} \end{bmatrix} \right\| \geq tol.$

In our implementation ¹, the gradient descent algorithm for the Tube loss kernel machine initially utilizes only the gradient of the Tube loss function. After a certain number of iterations, once we confirm that the upper bound of the PI, $K(A^T x_i)\alpha + b_1$, has moved above the lower bound, $K(A^T x_i)\alpha + b_2$, of PI, we incorporate the gradient of the PI tube width into the training of the Tube loss kernel machine.

Appendix C. Supplementary details of numerical experiments

Tuning r parameter:- Ideally, the tuning of the r parameter in the tube loss function should align with the skewness of the distribution $y|x$. However, real-world datasets often exist in high dimensions. Consequently, for a specific value of x , there may be only a few of y_i values in the training dataset, leading to potential inaccuracies in estimating the skewness of the distribution $y|x$. In practical benchmark experiments, we have tuned the r values for the tube loss machine from the set $\{0.1, 0.2, \dots, 0.9\}$.

Tuning δ parameter:- Initially, we initialize δ to zero in the Tube loss-based machine for benchmark dataset experiments and aim to achieve the narrowest PI by adjusting the r parameter, either moving the PI tube upwards or downwards. Once the r parameter is set and if the Tube loss-based machine achieves a coverage higher than the target t on the validation set, we gradually fine-tune the δ parameter from the set $\{0.001, 0.005, 0.1, 0.15, 0.2\}$ to minimize the tube width while maintaining the desired target coverage t .

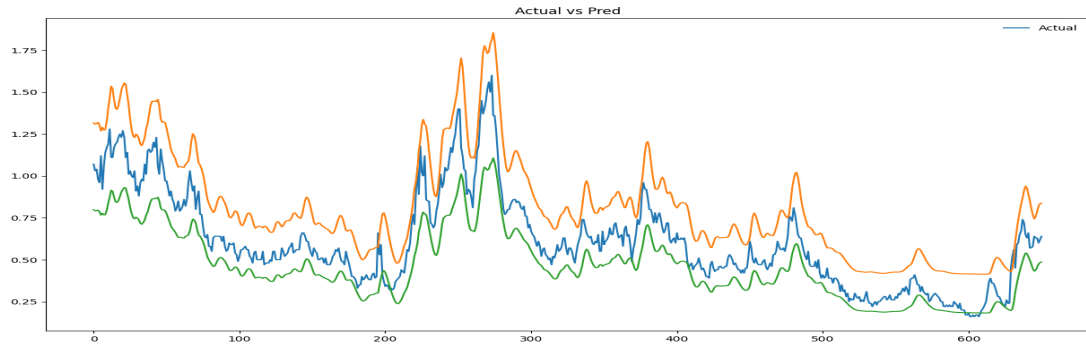
For generating the numerical results of Table 2, we have followed the experimental setup of Pearce et al. (2018). For the comparison of the tube loss function with the QD loss function, we have downloaded the code of QD loss experiments Pearce et al. (2018) available at https://github.com/TeaPearce/Deep_Learning_Prediction_Intervals/tree/master/code and plugged the tube loss function in it. For the Tube loss based NN model, r , δ , learning rate, decay rate and batch size were tuned for reporting the numerical results.

1. A MATLAB implementation of gradient descent with Tube loss is provided in supplementary material code.

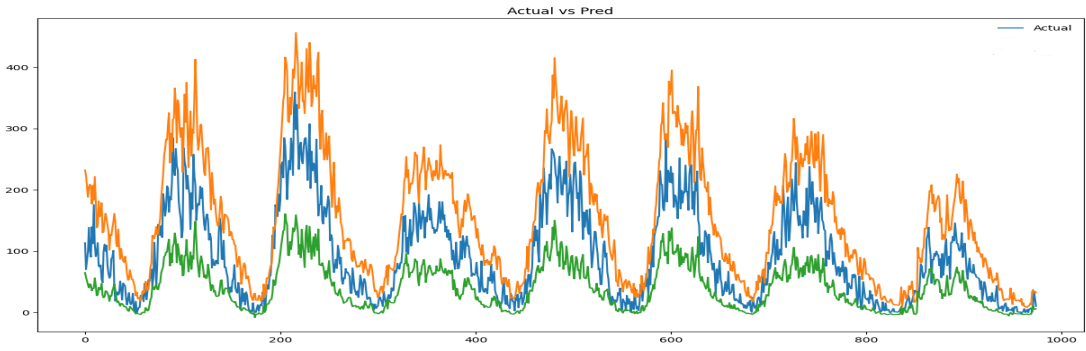
Dataset (Size)	LSTM Structure	Batch Size		Up,Low		Window Size	Learning Rate	
		Q- LSTM	T-LSTM	Q- LSTM	T-LSTM		Q-LSTM	T-LSTM
Sunspots (3265)	[256(0.3) ,128(0.2)]	128	128	0.98,0.03	0.5,0	16	0.001	0.001
Electric Production (397)	[64]	32	16	0.98,0.03	0.5,0.01	12	0.01	0.001
Daily Female Birth (365)	[100]	64	128	0.98,0.03	0.5,0.01	12	0.01	0.005
SWH (2170)	[128(0.4),64(0.3),32(0.2)]	300	300	0.98, 0.03	0.5, 0.01	100	0.001	0.001
Temperature (3651)	[16,8]	300	300	0.98, 0.03	0.5, 0.01	100	0.001	0.0001
Beer Production (464)	[64,32]	64	64	0.98, 0.03	0.1, 0.01	12	0.001	0.0001

Table 9: Tuned parameter values for Q-LSTM and T-LSTM model for considered benchmark datasets in Table 4. The LSTM architecture [128(0.4),64(0.3),32(0.2)] means that three hidden layers with neurons 128, 64 and 32 respectively and each hidden layer is followed by a drop out layer which are 0.4,0.3 and 0.2 respectively.

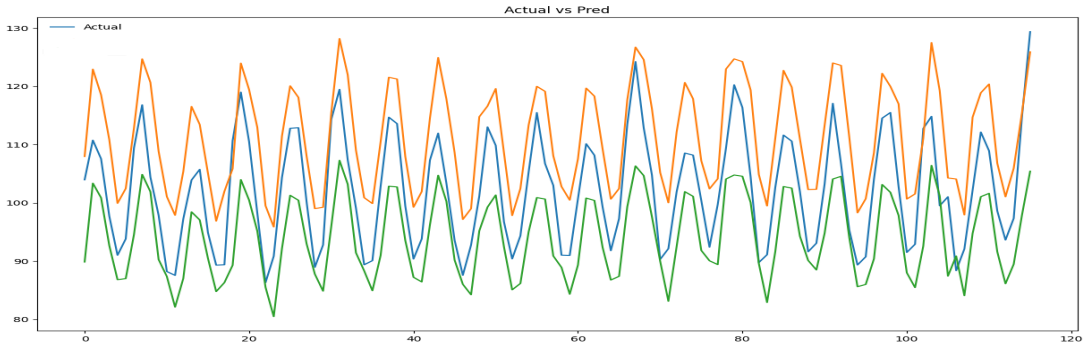
For QD loss based NN model, the optimal tuned parameters and numerical results were available. The Adam optimizer was used in both tube loss and QD loss based NN models.



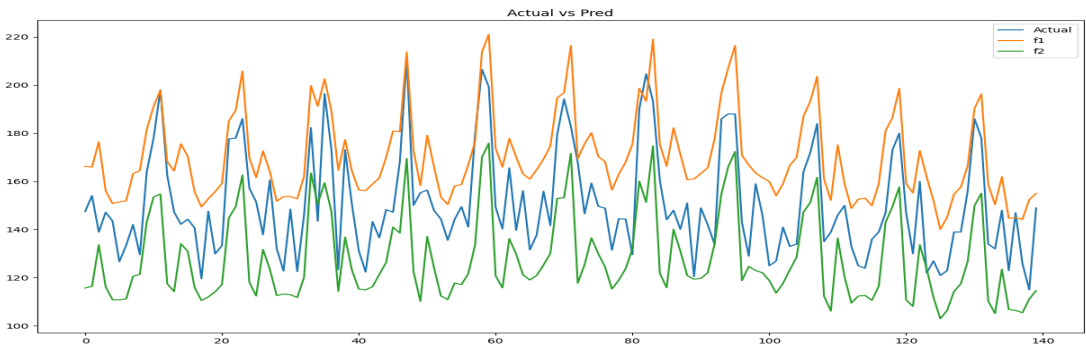
(a) SWH



(b) Sunspot



(c) Electric Production



(d) Beer Production

Figure 11: Probabilistic forecast of LSTM with proposed Tube loss function.

References

- Mousa Afrasiabi, Mohammad Mohammadi, Mohammad Rastegar, Lina Stankovic, Shahabodin Afrasiabi, and Mohammad Khazaei. Deep-based conditional probability density function forecasting of residential loads. *IEEE Transactions on Smart Grid*, 11(4):3646–3657, 2020.
- Anastasios N Angelopoulos, Rina Foygel Barber, and Stephen Bates. Theoretical foundations of conformal prediction. *arXiv preprint arXiv:2411.11824*, 2024.
- Parul Arora, Seyed Mohammad Jafar Jalali, Sajad Ahmadian, Bijaya K Panigrahi, Ponuthurai N Suganthan, and Abbas Khosravi. Probabilistic wind power forecasting using optimized deep auto-regressive recurrent neural networks. *IEEE Transactions on Industrial Informatics*, 19(3):2814–2825, 2022.
- Beer Production Australian. Beer production australian. <https://www.kaggle.com/datasets/sergiomora823/monthly-beer-production>, 1996. Accessed: 10-01-2024.
- BP and Ember. Electricity production by source (world). <https://www.kaggle.com/datasets/prateekmaj21/electricity-production-by-source-world>, 2016. Accessed: 10-01-2024.
- George Chryssolouris, Moshin Lee, and Alvin Ramsey. Confidence interval prediction for neural network models. *IEEE Transactions on neural networks*, 7(1):229–232, 1996.
- Youngseog Chung, Willie Neiswanger, Ian Char, and Jeff Schneider. Beyond pinball loss: Quantile methods for calibrated uncertainty quantification. *Advances in Neural Information Processing Systems*, 34:10971–10984, 2021.
- Mingjian Cui, Jie Zhang, Hongyu Wu, and Bri-Mathias Hodge. Wind-friendly flexible ramping product design in multi-timescale power system operations. *IEEE Transactions on Sustainable Energy*, 8(3):1064–1075, 2017.
- Peng Cui, Wenbo Hu, and Jun Zhu. Calibrated reliable regression using maximum mean discrepancy. *Advances in Neural Information Processing Systems*, 33:17164–17175, 2020.
- Wenkang Cui, Can Wan, and Yonghua Song. Ensemble deep learning-based non-crossing quantile regression for nonparametric probabilistic forecasting of wind power generation. *IEEE Transactions on Power Systems*, 38(4):3163–3178, 2022.
- datamarket.com. Daily total female births in california, 1959. <https://www.kaggle.com/datasets/dougcrewell/daily-total-female-births-in-california-1959>. Accessed: 10-01-2024.
- Shai Feldman, Stephen Bates, and Yaniv Romano. Improving conditional coverage via orthogonal quantile regression. *Advances in neural information processing systems*, 34:2060–2071, 2021.
- Azul Garza, Cristian Challu, and Max Mergenthaler-Canseco. Timegpt-1. *arXiv preprint arXiv:2310.03589*, 2023.

- Jan Gasthaus, Konstantinos Benidis, Yuyang Wang, Syama Sundar Rangapuram, David Salinas, Valentin Flunkert, and Tim Januschowski. Probabilistic forecasting with spline quantile function rnns. In *The 22nd international conference on artificial intelligence and statistics*, pages 1901–1910. PMLR, 2019.
- Jiani Heng, Yongmiao Hong, Jianming Hu, and Shouyang Wang. Probabilistic and deterministic wind speed forecasting based on non-parametric approaches and wind characteristics information. *Applied Energy*, 306:118029, 2022.
- Jianming Hu, Yingying Lin, Jingwei Tang, and Jing Zhao. A new wind power interval prediction approach based on reservoir computing and a quality-driven loss function. *Applied Soft Computing*, 92:106327, 2020a.
- Jianming Hu, Jingwei Tang, and Yingying Lin. A novel wind power probabilistic forecasting approach based on joint quantile regression and multi-objective optimization. *Renewable Energy*, 149:141–164, 2020b.
- JT Gene Hwang and A Adam Ding. Prediction intervals for artificial neural networks. *Journal of the American Statistical Association*, 92(438):748–757, 1997.
- HM Dipu Kabir, Abbas Khosravi, Mohammad Anwar Hosen, and Saeid Nahavandi. Neural network-based uncertainty quantification: A survey of methodologies and applications. *IEEE access*, 6:36218–36234, 2018.
- 1986 Karl Ulrich. Servo. <https://archive.ics.uci.edu/dataset/87/servo>, 2016. Accessed: 10-01-2024.
- Abbas Khosravi, Saeid Nahavandi, Doug Creighton, and Amir F Atiya. Lower upper bound estimation method for construction of neural network-based prediction intervals. *IEEE transactions on neural networks*, 22(3):337–346, 2011a.
- Abbas Khosravi, Saeid Nahavandi, Doug Creighton, and Amir F Atiya. Comprehensive review of neural network-based prediction intervals and new advances. *IEEE Transactions on neural networks*, 22(9):1341–1356, 2011b.
- Roger Koenker and Gilbert Bassett Jr. Regression quantiles. *Econometrica: journal of the Econometric Society*, pages 33–50, 1978.
- Roger Koenker and Kevin F Hallock. Quantile regression. *Journal of economic perspectives*, 15(4):143–156, 2001.
- machinelearningmastery.com. Daily minimum temperatures in melbourne. <https://www.kaggle.com/datasets/paulbrabban/daily-minimum-temperatures-in-melbourne>. Accessed: 10-01-2024.
- David JC MacKay. The evidence framework applied to classification networks. *Neural computation*, 4(5):720–736, 1992.
- Zhongxian Men, Eugene Yee, Fue-Sang Lien, Deyong Wen, and Yongsheng Chen. Short-term wind speed and power forecasting using an ensemble of mixture density neural networks. *Renewable Energy*, 87:203–211, 2016.

- James Mercer. Xvi. functions of positive and negative type, and their connection the theory of integral equations. *Philosophical transactions of the royal society of London. Series A, containing papers of a mathematical or physical character*, 209(441-458):415–446, 1909.
- NDBC. Significant wave height, national data buoy center, buoy station 42001 for 21 april 2021 - 25 july 2021. https://www.ndbc.noaa.gov/station_history.php?station=42001.
- David A Nix and Andreas S Weigend. Estimating the mean and variance of the target probability distribution. In *Proceedings of 1994 ieee international conference on neural networks (ICNN'94)*, volume 1, pages 55–60. IEEE, 1994.
- Hossein Panamtaash and Qun Zhou. Coherent probabilistic solar power forecasting. In *2018 IEEE International Conference on Probabilistic Methods Applied to Power Systems (PMAPS)*, pages 1–6. IEEE, 2018.
- Georgios Papadopoulos, Peter J Edwards, and Alan F Murray. Confidence estimation methods for neural networks: A practical comparison. *IEEE transactions on neural networks*, 12(6):1278–1287, 2001.
- Harris Papadopoulos. Inductive conformal prediction: Theory and application to neural networks. In *Tools in artificial intelligence*. Citeseer, 2008.
- Tim Pearce, Alexandra Brintrup, Mohamed Zaki, and Andy Neely. High-quality prediction intervals for deep learning: A distribution-free, ensembled approach. In *International conference on machine learning*, pages 4075–4084. PMLR, 2018.
- Yaniv Romano, Evan Patterson, and Emmanuel Candes. Conformalized quantile regression. *Advances in neural information processing systems*, 32, 2019.
- Adnan Saeed, Chaoshun Li, and Zhenhao Gan. Short-term wind speed interval prediction using improved quality-driven loss based gated multi-scale convolutional sequence model. *Energy*, 300:131590, 2024.
- Tárik S Salem, Helge Langseth, and Heri Ramampiaro. Prediction intervals: Split normal mixture from quality-driven deep ensembles. In *Conference on Uncertainty in Artificial Intelligence*, pages 1179–1187. PMLR, 2020.
- David Salinas, Valentin Flunkert, Jan Gasthaus, and Tim Januschowski. Deepar: Probabilistic forecasting with autoregressive recurrent networks. *International journal of forecasting*, 36(3):1181–1191, 2020.
- SIDC and Quandl. Sunspots. <https://www.kaggle.com/datasets/robervalt/sunspots>. Accessed: 10-01-2024.
- Ichiro Takeuchi, Quoc Le, Timothy Sears, Alexander Smola, et al. Nonparametric quantile estimation. 2006.
- Lyle H Ungar, Richard D De Veaux, and Evelyn Rosengarten. Estimating prediction intervals for artificial neural networks. In *Proc. of the 9th yale workshop on adaptive and learning systems*, 1996.

- Vladimir Vovk, Alexander Gammerman, and Glenn Shafer. *Algorithmic learning in a random world*, volume 29. Springer, 2005.
- Volodya Vovk, Alexander Gammerman, and Craig Saunders. Machine-learning applications of algorithmic randomness. 1999.
- Can Wan, Jin Lin, Jianhui Wang, Yonghua Song, and Zhao Yang Dong. Direct quantile regression for nonparametric probabilistic forecasting of wind power generation. *IEEE Transactions on Power Systems*, 32(4):2767–2778, 2016.
- Yi Wang, Dahua Gan, Mingyang Sun, Ning Zhang, Zongxiang Lu, and Chongqing Kang. Probabilistic individual load forecasting using pinball loss guided lstm. *Applied Energy*, 235:10–20, 2019.
- Chongchong Xu and Guo Chen. Interpretable transformer-based model for probabilistic short-term forecasting of residential net load. *International Journal of Electrical Power & Energy Systems*, 155:109515, 2024.
- Luoxiao Yang, Zhong Zheng, and Zijun Zhang. An improved mixture density network via wasserstein distance based adversarial learning for probabilistic wind speed predictions. *IEEE Transactions on Sustainable Energy*, 13(2):755–766, 2021.
- Yixiao Yu, Ming Yang, Xueshan Han, Yumin Zhang, and Pingfeng Ye. A regional wind power probabilistic forecast method based on deep quantile regression. *IEEE Transactions on Industry Applications*, 57(5):4420–4427, 2021.
- Hao Zhang, Yongqian Liu, Jie Yan, Shuang Han, Li Li, and Quan Long. Improved deep mixture density network for regional wind power probabilistic forecasting. *IEEE Transactions on Power Systems*, 35(4):2549–2560, 2020.
- Wenjie Zhang, Hao Quan, and Dipti Srinivasan. An improved quantile regression neural network for probabilistic load forecasting. *IEEE Transactions on Smart Grid*, 10(4):4425–4434, 2018.
- Jianhua Zhu and Yaoyao He. A large-scale multi-objective evolutionary quantile estimation model for wind power probabilistic forecasting. *IEEE Transactions on Evolutionary Computation*, 2024.
- Zhenglin Zhu, Yusen Xu, Junzhao Wu, Yiwen Liu, Jianwei Guo, and Haixiang Zang. Wind power probabilistic forecasting based on combined decomposition and deep learning quantile regression. *Frontiers in Energy Research*, 10:937240, 2022.